# NUMERICAL STUDY OF PLANE WAVE SCATTERING FROM CYLINDRICAL CAVITY BACKED APERTURES WITH OUTER OR INNER MATERIAL COATING

A THESIS

SUBMITTED TO THE DEPARTMENT OF ELECTRICAL AND
ELECTRONICS ENGINEERING
AND THE INSTITUTE OF ENGINEERING AND SCIENCES
OF BILKENT UNIVERSITY
IN PARTIAL FULFILLMENT OF THE REQUIREMENTS
FOR THE DEGREE OF
MASTER OF SCIENCE

By
Dilek Çolak
July, 1993

# NUMERICAL STUDY OF PLANE WAVE SCATTERING FROM CYLINDRICAL CAVITY-BACKED APERTURES WITH OUTER OR INNER MATERIAL COATING

A THESIS

SUBMITTED TO THE DEPARTMENT OF ELECTRICAL AND

ELECTRONICS ENGINEERING

AND THE INSTITUTE OF ENGINEERING AND SCIENCES

OF BILKENT UNIVERSITY

IN PARTIAL FULFILLMENT OF THE REQUIREMENTS

FOR THE DEGREE OF

MASTER OF SCIENCE

By

Dilek Çolak

July 1993

I certify that I have read this thesis and that in my opinion it is fully adequate, in scope and in quality, as a thesis for the degree of Master of Science.

Assoc. Prof. Dr. Ayhan Altıntaş(Principal Advisor)

I certify that I have read this thesis and that in my opinion it is fully adequate, in scope and in quality, as a thesis for the degree of Master of Science.

Assoc. Prof. Dr. Alexander I. Nosich

I certify that I have read this thesis and that in my opinion it is fully adequate, in scope and in quality, as a thesis for the degree of Master of Science.

Assis. Prof. Dr. Gönül (Turhan) Sayan
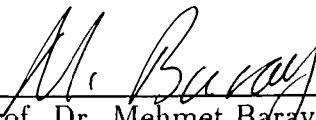
I certify that I have read this thesis and that in my opinion it is fully adequate, in scope and in quality, as a thesis for the degree of Master of Science.

Assoc. Prof. Dr. Merih Büyükdura

Approved for the Institute of Engineering and Sciences:

Prof. Dr. Mehmet Baray
Director of Institute of Engineering and Sciences

ii

# ABSTRACT

## NUMERICAL STUDY OF PLANE WAVE SCATTERING FROM CYLINDRICAL CAVITY-BACKED APERTURES WITH OUTER OR INNER MATERIAL COATING

Dilek Çolak
M.S. in Electrical and Electronics Engineering
Supervisors: Assoc. Prof. Dr. Ayhan Altıntaş
July 1993

In this thesis, a dual-series-based solution is obtained for the scattering of a time harmonic plane wave from a cavity-backed aperture(CBA) which is formed by a slitted infinite circular cylinder coated with absorbing material. The material coating can be done on the inner or outer surface of the cylinder. For both cases, numerical results are presented for the radar cross section (RCS) and comparisons of the suppression of RCS are given for two different realistic absorbing materials. Finally, the dependence of RCS on the thickness of the absorbing layer and on the aspect angle of the screen are presented numerically. To the best of our knowledge, this is the first study made so far to solve the problems of CBAs with material coating inside or outside with this approach.

*Keywords :* Radar Cross Section (RCS), cavity-backed aperture (CBA), Riemann-Hilbert problem (RHP), Electromagnetic Scattering, Dual-Series Equations.

# ÖZET

## DUVARLARI İÇTEN VEYA DIŞTAN KAPLANILMIŞ MAĞARALI AÇIKLIKLARDAN ELEKTROMANYETİK SAÇINIM PROBLEMİNİN NÜMERİK ANALİZİ

Dilek Çolak
Elektrik ve Elektronik Mühendisliği Bölümü Yüksek Lisans
Tez Yöneticisi:   Doç. Dr. Ayhan Altıntaş
Temmuz 1993

Bu tezde, iki boyutlu ve yüzleri yalıtkan maddeyle kaplı, yanı açık iletken silindirden elektromanyetik saçınım problemi, Riemann-Hilbert yöntemiyle incelendi. Radar kesit sonuçları, kovuk duvarlarının içerden ya da dışardan kaplanmasına göre, değişik malzemelere göre elde edildi, ve sonuçlar kendi aralarında karşılaştırıldı. Ayrıca, degişik silindir yarıçapları, kaplama malzemesinin kalınlığı, gelen dalganın frekansı, değişik gelme açıları gibi parametrelerin sonuca etkileri araştırıldı. Riemann-Hilbet problemi yöntemi ile, içerisi veya dışarısı malzeme kaplı kovuklu açıklıklardan saçınım probleminin çözümüne literatürde daha önce rastlanmamıştır.

*Anahtar Kelimeler :* Radar kesidi, kovuklu açıklık, Riemann-Hilbert problemi (RHP), Elektromanyetik Saçınım, İkil seri denklemleri.

# ACKNOWLEDGEMENT

# TABLE OF CONTENTS

# LIST OF FIGURES

# Chapter 1

# INTRODUCTION

Cavity-backed apertures (CBA) are encountered as parts of any airborne or spaceborne radar targets. Most familiar of them are, probably, air inlets and engine tubes, known to contribute a great deal to radar cross section of jet aircraft. What is even more dangerous, the CBAs are famous for the internal resonances, which can easily result in recognizing the shape of a target. More often than not, these effects are considered as undesired and are to be suppressed. To this end, the walls of the cavity are covered with some lossy material.

The problem of electromagnetic wave scattering from partially open cylindrical and spherical cavities have been studied extensively in the literature. To simulate the scattering from these CBA geometries, two dimensional (2-D) and three dimensional (3-D) models of open-ended waveguide-type cavities are usually employed. Absorption for thin coatings is generally modeled by introducing boundary conditions of impedance type. In the papers [1–6], the scattering from such cavities is treated by various approximate asymptotic approaches, such as Geometrical Theory of Diffraction (GTD), Uniform Theory of Diffraction (UTD), bouncing ray and hybrid methods (modal and ray approaches). The simplicity and physical appeal of these high frequency approaches are not complemented by the clear limits of accuracy. Besides, it is principally difficult to take into account various parts of the scatterer and their interaction with uniform accuracy. Also, the mentioned high frequency approaches fail for cavities with dimensions comparable to the wavelength. A Wiener-Hopf-based approach to solve similar 2-D problems for unloaded and

loaded rectangular CBA [7] is free of these difficulties. But, it becomes cumbersome if the walls of the cavity are covered with absorbers. In a recent study [8], the multiple parameter perturbation analysis has been applied to the slitted loaded cavity problem comprising two eccentric circular cylinders. Mautz and Harrington proposed a generalized network formulation [9] and applied this method to solve circular cylindrical shell with an infinitely long slot [10]. The same problem has also been treated in [11] by using characteristic mode theory and in [25] by using three different methods, i.e., aperture field integral equation, H-field and E-field integral equation. The discussion on the comparative advantages of different techniques is still continuing (see [11] and the list of references).

For certain canonical geometries, there exists an accurate approach of analytical numerical nature which ensures any desired accuracy of the obtained results. This is the dual-series-based Riemann-Hilbert Problem (RHP) approach of complex variable theory. It has been under intensive study in the former USSR since the 1960's [12]. In the 70's and 80's large amount of results have been obtained on free-space scattering from open screens and collections of screens (see [13] and the cited literature). This approach has been utilized to solve the problem of plane wave scattering from an infinitely long circular cylinder with a longitudinal slot by Nosich [14]. In the West the dual-series-based approach was exploited by Ziolkowski [16]–[15]. It was unfortunate that a numerical error was present in [17] for E-case (reported in [20]), which obviously should not discredit the method. Actually, correct RHP-based RCS analysis results were published in [21], but remained unknown for Western readers.

The main advantage of the dual-series-based approach is that it is based on the idea of partial analytical inversion of the scattering operator. Final matrix equations are proven to be of the Fredholm 2nd kind, so the solution exists and it can be approximated through truncation.

In present study, the dual-series-based RHP technique has been extended to solve the problems of CBAs with material coating inside or outside. Our canonical geometry is a circular shell formed by a zero-thickness, perfectly-conducting screen having an opening. An arbitrarily-thin lossy homogeneous material can be introduced as a concentric layer on either inner or outer surface of the shell, [22]. We do realize that this 2-D model geometry is far from a real jet inlet. Nevertheless such a scatterer exhibits resonant behavior of quite a general nature. Studying this behavior and the effect of absorber in details, one

2

can judge about more realistic geometries. Another important thing is that, the method is equally effective for any angular width of the shell from 0 to $2\pi$. The size of the matrix is determined by the electrical radius of curvature, and fairly large structures can be treated accurately.

E-wave and H-wave excitation results are considered. Unlike the E-polarized case, there appear a low frequency spike in RCS for the H-polarized case which does not correspond to any interior resonance of the closed cavity. This resonance is called quasi-static or slot-mode, as the corresponding electric field is concentrated at the slot. Nosich has shown that this resonance is similar to the Helmholtz resonance known in acoustics [19]. The location of this spike is found from approximate solution of exact eigenfrequency equation in [19], and also from an equivalent LC circuit in the vicinity of the slot in [17], [19], [23], and [24]. Since the wall current in H-polarized case flows in circumferential direction, there appears oscillations in RCS pattern even for closed cylinder case, which is not case in E-polarized excitation.

Although we have considered only circular cylindrical cavities, the numerical data obtained can obviously bring a better understanding of the scattering behavior of loaded cavities. It can also serve as a reference data for checking numerical codes for more complicated scatterers, e.g. solved by method of moments [23], [24], [25].

The outline of this thesis as follows: In Chapter 2, a brief explanation of the theory of analytical functions of complex variable and Cauchy type integrals are given, and then the method of solution for canonical dual series equations is presented. In the third Chapter, the problem is formulated, and then solved via RHP technique for both polarizations. Sample numerical results and discussions on the results are presented in Chapter 4. Finally, some conclusions are given in Chapter 5.

# Chapter 2

# MATHEMATICAL PRELIMINARIES FOR THE METHOD

The Riemann-Hilbert problem technique of complex variable theory makes it possible to obtain analytical solutions to canonical wave scattering and diffraction problems. Examples of canonical problems solvable with this technique include a plane wave incidence on a circular cylinder with an infinite axial slot and with multiple infinite axial slots, on diffraction grating of plane strips and on a slitted cone. Due to periodicity of boundaries, all the problems can be rearranged in the form of dual series equations with the set of functions $e^{in\varphi}$, $n = 0, \mp 1, \cdots$ as the kernel.

In this chapter, a brief explanation on the theory of analytical functions of complex variable and Cauchy type integrals is given, since Riemann-Hilbert problem is concerned with finding an analytical function that satisfies a prescribed transition condition on an open or closed curve. And, the method of solution for canonical dual series equations is presented in the last section of this chapter.

## 2.1 Riemann-Hilbert Problem in the Complex Variable Theory

Consider a simple closed, smooth curve L which divides the complex plane into two domains $Q^{\mp}$ such that $Q^+ = extL$ and $Q^- = intL$. Let X(z) be a sectionally analytic function such that $X(z) = X^{\mp}(z)$ for $z \in Q^{\mp}$. If we assume that X(z) vanishes at infinity, and also satisfies the transition condition

$$X^+(z_o) - X^-(z_o) = B(z_o), \quad z_o \in L \tag{2.1}$$

with at least Hölder continuous function of position on that contour, and B($z_o$) is a known function usually denoted as the free term, then the Cauchy integral

$$X(z) = \frac{1}{2\pi i} \int_L \frac{B(z_o)}{(z_o - z)} dz_o \tag{2.2}$$

gives the solution. For such integrals, the Plemelj-Sokhotskii formulas [29] are valid

$$X^{\mp}(z_o) = X(z_o) \mp \frac{1}{2} B(z_o) \ . \tag{2.3}$$

The RHP is a generalized version of this problem. Another known function $A(z_o)$ is also introduced which is also Hölder continuous function on the curve L, such that X(z) satisfies the following transition condition

$$X^+(z_o) - A(z_o)X^-(z_o) = B(z_o) \ . \tag{2.4}$$

A further generalization of this problem is possible by introducing discontinuous coefficients, $A(z_o)$ and $B(z_o)$ in (2.4). In addition, the behavior of X(z) at infinity can also be modified. For instance, it may also be described by a polynomial function of z. Let, the curve L be divided into two sets, M and S, such that $M \bigcup S = L$, as shown in Figure 2.1. Consider a boundary value problem of finding an analytic function X(z) with the boundary expressions

$$X^+(z_o) + X^-(z_o) = B(z_o), \quad z_o \in M,$$

$$X^+(z_o) - X^-(z_o) = 0 \qquad z_o \in S \ . \tag{2.5}$$

The two equations in (2.5) can be rearranged as a single one as

$$X^+(z_o) - \tilde{A}(z_o)X^-(z_o) = \tilde{B}(z_o) \tag{2.6}$$

5
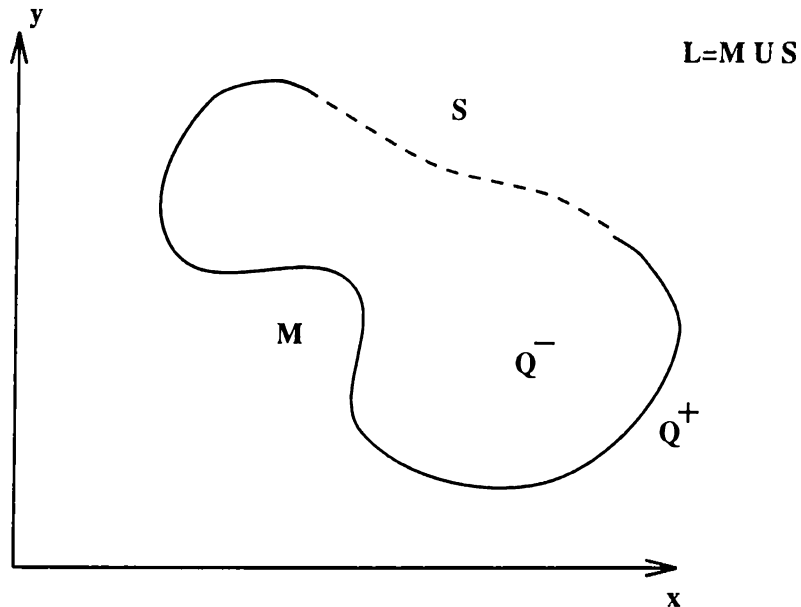
Figure 2.1: Simple closed curve on the complex plane

by introducing discontinuous coefficient and free term functions

$$\tilde{A}(z_o) = \begin{cases} -1, & z_o \in M \\ +1, & z_o \in S \end{cases} \quad , \quad \tilde{B}(z_o) = \begin{cases} B(z_o), & z_o \in M \\ 0, & z_o \in S \end{cases} \quad (2.7)$$

Note that equation (2.6) is valid on the whole closed contour L.

To make further derivations, it is necessary to specify the behavior of the unknown function X(z) at infinity and at the end points of the open curve M where $\tilde{A}(z)$ and $\tilde{B}(z)$ becomes discontinuous. It is assumed that X(z) has singularities of order $1/2$ at each of the end points and is zero at infinity, which is a typical behavior for the electromagnetics problems of wave scattering and diffraction by perfectly conducting zero thickness slitted cylinders. However, the RHP technique can actually handle solutions with other singularities of the order less than 1, with nonzero behavior at infinity, [29].

## 2.2 Solution of the Riemann-Hilbert Problem

By making the assumptions introduced in the previous section, we can define a function R(z), which is also called characteristic function, such that the

multiplication of R(z) with X(z) becomes nonsingular everywhere, i.e. regular on the whole complex plane [29]. It is given as

$$R(z) = (z - \alpha_1)^{1/2}(z - \alpha_2)^{1/2} \tag{2.8}$$

where $z = \alpha_{1,2}$ are the endpoints, and the branch is chosen such that brunch-cut is from $\alpha_1$ to $\alpha_2$ along S. Then the limit values as $z \to z_o \in S$ of R(z) differ by sign, i.e. $R(z) \to R^{\mp}(z_o) = \mp R^{+}(z_o)$.

By introducing functions Y(z) and $D(z_o)$ such that

$$Y(z) = X(z)R(z)$$

$$D(z_o) = \tilde{B}(z_o)R^{+}(z_o) \tag{2.9}$$

we come to a RHP with continuous coefficient function on the closed curve L

$$Y^{+}(z_o) - Y^{-}(z_o) = D(z_o) \ . \tag{2.10}$$

Since the characteristic function has a simple pole at infinity, the solution of (2.10) is given as [29]

$$Y(z) = \frac{1}{2\pi i} \int_L \frac{D(z_o)}{(z_o - z)} \, dz_o + C \ . \tag{2.11}$$

The equation (2.11) can be written for the function X(z)

$$X(z) = \frac{1}{2\pi i} \frac{1}{R(z)} \int_M \frac{R^{+}(z_o)B(z_o)}{(z_o - z)} \, dz_o + \frac{C}{R(z)} \tag{2.12}$$

which is the exact solution of the initial Riemann-Hilbert problem (2.5) with the restricted behavior of X(z) at the infinity and at the endpoints of the curve M. Because of the singular character of the integral on the right hand part of (2.12), this solution is not much effective computationally. The unknown constant C on the right hand can usually be obtained due to certain additional conditions from the physical nature of the initial problem which is converted to RHP.

7

## 2.3 Solution of Canonical Dual Series Equations

Consider the dual series equations with trigonometric kernel for the infinite sequence of coefficients $x_n$, $n = 0, \mp 1, \cdots$ is given as

$$\sum_{n=-\infty}^{\infty} x_n \mid n \mid e^{in\varphi} = F(e^{i\varphi}), \qquad \varphi \in S = \mid \varphi \mid < \theta \qquad (2.13)$$

$$\sum_{n=-\infty}^{\infty} x_n e^{in\varphi} = 0, \qquad \varphi \in M = (\theta < \mid \varphi \mid \leq \pi) \ . \qquad (2.14)$$

These dual series equations can be solved by converting the problem into a Riemann-Hilbert problem. Assuming that the series in (2.14) is term-by-term differentiable, we replace it with the derivative with respect to $\varphi$. Then we have the following equations

$$\sum_{n=-\infty}^{\infty} x_n \mid n \mid e^{in\varphi} = F(e^{i\varphi}), \ \ \text{on S}$$

$$\sum_{n=-\infty}^{\infty} x_n n e^{in\varphi} = 0, \qquad \text{on M} \qquad (2.15)$$

$$\sum_{n=-\infty}^{\infty} x_n e^{in\pi} = 0 \ \ .$$

The last equation is obtained by substituting $\varphi = \pi$ into (2.14) to account for the elimination of the constant term due to differentiation.

By introducing functions $X^{\mp}(z)$ of complex variable $z = re^{i\varphi}$ such that

$$X^{+}(z) = + \sum_{n=1}^{\infty} x_n n z^n, \ \ \text{analytic in } Q^{+}, \text{ and } \mid z \mid < 1$$

$$X^{-}(z) = - \sum_{n=-\infty}^{-1} x_n n z^n, \ \ \text{analytic in } Q^{-}, \text{ and } \mid z \mid > 1 \qquad (2.16)$$

we obtain a functional equation valid on the whole unit circle $\mid z \mid = 1$

$$X^{+}(e^{i\varphi}) - AX^{-}(e^{i\varphi}) = B \qquad (2.17)$$

with known, however, discontinuous coefficient and free term functions

$$A(\varphi) = \begin{cases} -1, & \text{on S} \\ +1, & \text{on M} \end{cases}, \quad B(\varphi) = \begin{cases} F(e^{i\varphi}), & \text{on S} \\ 0, & \text{on M} \end{cases} \quad (2.18)$$

To arrive at the exact solution of (2.17), it is necessary to restrict the behavior of the unknown function $X(z)$ at the infinity and at the end points of the screen. By assuming that $X(z)$ vanishes as $|z| \to \infty$, and has a square root singularity at the endpoints, $z = e^{\mp i\theta}$, the solution is given by the equation (2.12). By using Plemelj-Sokhotskii formulas [29] for the limiting values of the $X(z)$, we obtain

$$X^+(t_o) - X^-(t_o) = \frac{Q(t_o)}{i\pi} \int_S \frac{R^+(t)F(t)}{(t-t_o)} \, dt + 2CQ(t_o) \quad (2.19)$$

where $t, t_o \in L$ and

$$Q(t_o) = \begin{cases} [R^+(t_o)]^{-1}, & t_o \in S \\ 0, & t_o \in M \end{cases}$$

The definition in (2.16) yields

$$X^+(t_o) - X^-(t_o) = \sum_{(n)} n x_n e^{in\varphi} \quad . \quad (2.20)$$

By taking the Fourier inversion of (2.20), we obtain

$$m x_m = V_m(F, \theta) + 2C R_m(\theta), \quad m = 0, \mp 1, \cdots \quad (2.21)$$

where

$$V_m(F, \theta) = \frac{1}{2\pi} \int_0^{2\pi} Q(e^{i\psi_o}) V(F, e^{i\psi_o}) e^{-im\psi_o} \, d\psi_o = \frac{1}{2\pi} \int_M \frac{V(F, e^{i\psi_o}) e^{-im\psi_o}}{R^+(e^{i\psi_o})} \, d\psi_o$$

$$V(F, e^{i\psi_o}) = \frac{1}{i\pi} P.V. \int_M \frac{R^+(t)F(t)}{t - e^{i\psi_o}} \, dt$$

$$R_m(\cos\theta) = \frac{1}{2\pi} \int_0^{2\pi} Q(e^{i\psi_o}) e^{-im\psi_o} \, d\psi_o = \frac{1}{2\pi} \int_M \frac{e^{-im\psi_o}}{R^+(e^{i\psi_o})} \, d\psi_o$$

9

The constant term in (2.19) can be found by setting $m = 0$ in (2.21) as

$$C = -\frac{V_o}{2R_o} \tag{2.22}$$

Assuming that the free term function has the Fourier expansion as

$$F(e^{i\psi}) = \sum_{(n)} f_n e^{i\psi n} \ , \tag{2.23}$$

one can obtain

$$V_m(F, \theta) = \sum_{(n)} f_n V_m^n \tag{2.24}$$

where

$$V_m^n = \frac{1}{2\pi} \int_M \frac{v_n(e^{i\psi_o}, \theta)}{R^+(e^{i\psi_o})} e^{-im\psi_o} \, d\psi_o \tag{2.25}$$

$$v_n(t_o, \theta) = \frac{1}{i\pi} P.V. \int_M \frac{R^+(t)t^n}{t - t_o} \, dt \ . \tag{2.26}$$

Therefore, the equation in (2.19) can be reduced to

$$x_m m = \sum_{(n)} f_n \tilde{V}_m^n \tag{2.27}$$

where

$$\tilde{V}_m^n = V_m^n - V_o^n \frac{R_m}{R_o} \ .$$

From the last equation in (2.15), one can find $x_o$ as

$$x_o = -\sum_{(n)} f_n \sum_{(m \neq 0)} (-1)^m \frac{\tilde{V}_m^n}{m} \ . \tag{2.28}$$

The calculation of $v_n$, $V_m^n$ and $R_m$ requires a fine technique of integration in the complex plane and it was performed by Agranovich *et. al.* [12]. In terms of Legendre polynomials $P_n(cos\theta)$ the results are as follows

$$V_m^n(\cos\theta) = \frac{m+1}{2(m-n)}[P_m(\cos\theta)P_{n+1}(\cos\theta) - P_{m+1}(\cos\theta)P_n(\cos\theta)]$$

$$R_m(\cos\theta) = \frac{1}{2}P_m(\cos\theta), \qquad \tilde{V}_m^n = V_{m-1}^{n-1} \tag{2.29}$$

$$\sum_{m \neq 0}(-1)^m \frac{V_{m-1}^{n-1}(\cos\theta)}{m} = \begin{cases} -\frac{1}{n}V_{n-1}^{-1}(\cos\theta), & n \neq 0 \\ \ln\frac{1+\cos\theta}{2} & n = 0 \end{cases}$$

10

The final solution to the Riemann-Hilbert problem is found as

$$x_m = \sum_{(n)} f_n T_{mn}(\cos\theta) \tag{2.30}$$

where

$$T_{mn}(\cos\theta) = \begin{cases} \frac{1}{m} V_{m-1}^{n-1}(\cos\theta), & m \neq 0 \\ \frac{1}{n} V_{n-1}^{-1}(\cos\theta), & m = 0,\ n \neq 0 \\ -\ln\frac{1+\cos\theta}{2}, & m = n = 0 \end{cases} \tag{2.31}$$

# Chapter 3

# SCATTERING FROM CAVITY-BACKED APERTURES WITH MATERIAL COATING

The problem of electromagnetic scattering of a time harmonic plane wave from a thin, perfectly conducting, slitted infinite cylinder which is coated with absorbing material either from inside or from outside is analyzed in this chapter. The formulation of the problem is given in the first section. The dual-series equations are derived and then solved via RHP approach in the following two sections. The time dependence $e^{-iwt}$ has been assumed and suppressed.

## 3.1 Formulation of the Problem

The geometries analyzed in this thesis are shown in Figures 3.1 and 3.2. The coordinate system $(r,\varphi,z)$ is coaxial with the cylinder. The plane wave is assumed to be normally incident on the cylinder; hence the problem is two dimensional. Two types of polarization for the incident plane wave are considered separately. For the transverse magnetic polarization (E-polarization), the incident E-field is parallel to the axis. For the transverse electric polarization (H-polarization),
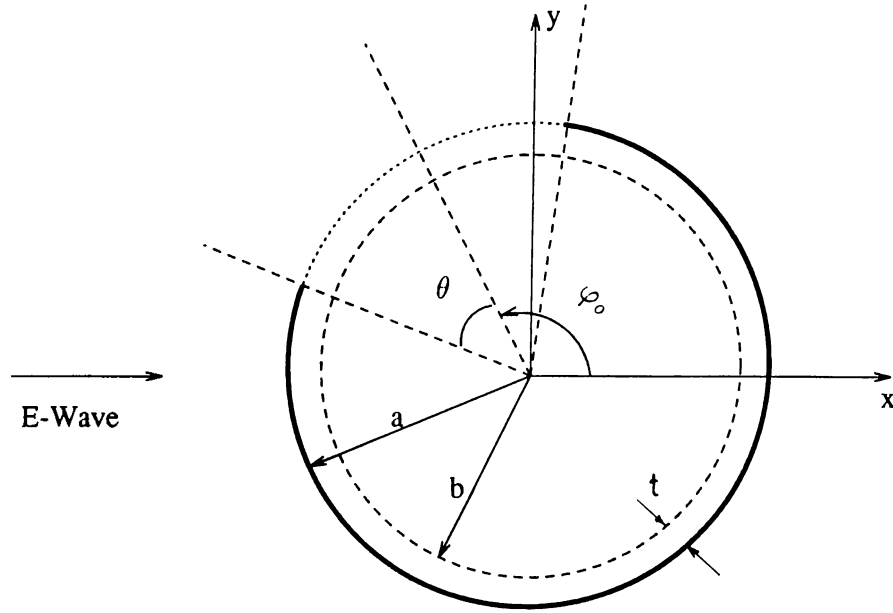
Figure 3.1: Plane wave scattering by an inner-coated cavity-backed aperture

the incident H-field is parallel to the axis. The screen which has a radius of "$a$" is taken to be in the interval of $\theta <| \varphi - \varphi_o |\leq \pi$. Angular width of the slit is $2\theta$, and the angle between the center of the slit and the $x$ axis is $\varphi_o$. The cylindrical cavity is coated with absorbing material with a thickness $t$. The radius "$b$" is at either $a - t$ or $a + t$ depending on whether the coating is on the inside or on the outside, respectively. The relative permittivity and permeability of the absorbing material are $\epsilon_r$ and $\mu_r$, respectively. Our objective is to analyze the radar scattering behavior of this geometry for various frequencies. The problem is scalar, so the total field can be characterized by the single $U_z$ component.

First, consider the geometry shown in Figure 3.1. The total field can be expressed as follows

$$
U_z(\vec{r}) = \begin{cases} U_z^{in}(\vec{r}) + U_z^{sc}(\vec{r}), & r > a \\ U_z^{sc}(\vec{r}), & b < r < a \\ U_z^{sc}(\vec{r}), & r < b \end{cases} \tag{3.1}
$$

where $U_z^{in}$ and $U_z^{sc}$ stand for incident and scattered fields, respectively.

The scattered field $U_z^{sc}$ satisfies the 2-D Helmholtz equations:

$$
\begin{aligned}
(\nabla^2 + k_o^2 \quad )U_z^{sc}(\vec{r}) = 0, & \quad r > a, \ r < b \\
(\nabla^2 + k_o^2 \epsilon_r \mu_r )U_z^{sc}(\vec{r}) = 0, & \quad b < r < a
\end{aligned} \tag{3.2}
$$

13
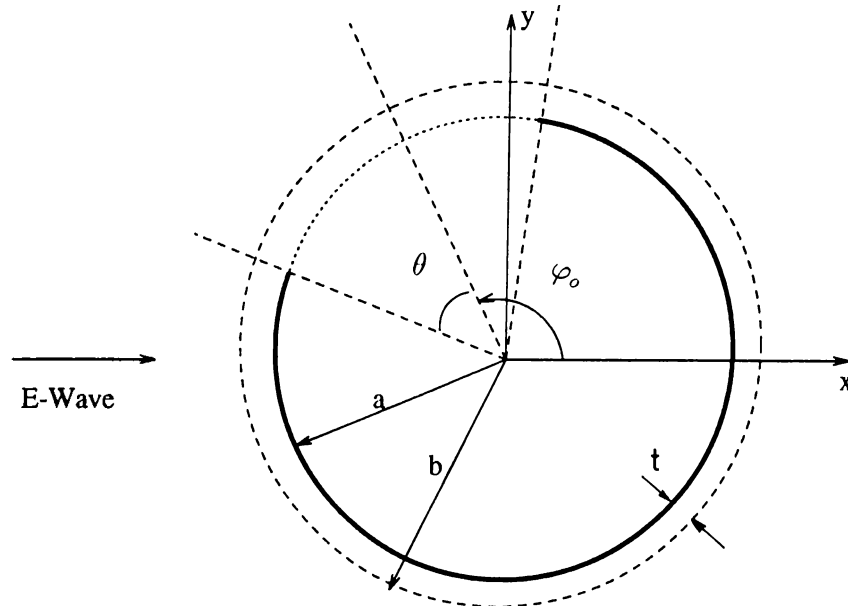
Figure 3.2: Plane wave scattering by an outer-coated cavity-backed aperture

where $k_o = \omega\sqrt{\mu_o\epsilon_o}$ is the free-space wave number and $\nabla^2$ is the Laplacian operator in 2-D.

In addition, we impose the boundary conditions: $U_z$ and its radial derivatives should satisfy

$$[U_z] = 0, \tag{3.3}$$

$$\left[\delta\frac{\partial U_z}{\partial r}\right] = 0 \tag{3.4}$$

respectively, with

$$\delta = \begin{cases} \frac{1}{\mu} & \text{for E-pol} \\ \frac{1}{\epsilon} & \text{for H-pol} \end{cases}$$

on the closed contour $r = b$. The square brackets in (3.3) and (3.4) denote the jump of the field function on the specified contour. The electric field is continuous on the closed contour $r = a$ which imposes either (3.3) for E-pol. or (3.4) for H-pol. to be valid. In addition, magnetic field is continuous at the aperture, $| \varphi - \varphi_o | < \theta$, implies that (3.4) for E-pol and (3.3) for H-pol. are to be employed. Besides, the electric field must vanish on the screen, i.e., depending on the type of the polarization of the incident field, either $U_z$ (for E-pol) or its derivative with respect to $r$ (for H-pol) vanishes on the screen.

Because of the sharp edges of the screen, the field should satisfy certain edge conditions. The total electrical and magnetic energy stored inside any

14

finite neighborhood of the edge is limited, i.e.,

$$\int_B (k_o^2 \mid U_z^{sc} \mid^2 + \mid \nabla U_z^{sc} \mid^2) \, d\vec{r} < \infty \qquad (3.5)$$

where $B$ is any bounded domain around the edge. Finally, the Sommerfeld radiation condition

$$U_z^{sc}(\vec{r}) \sim \Phi(\varphi) \left( \frac{2}{i\pi k_o r} \right)^{1/2} e^{ik_o r} \qquad (3.6)$$

should be satisfied far from the scatterer as $r \to \infty$.

## 3.2    Derivation of Dual Series Equations

The scattered field expansions in three regions of Figure 3.1 are assumed to be

$$U_z^{sc} = \sum_{n=-\infty}^{\infty} \left\{ \begin{array}{ll} A_n H_n(k_o r) & r > a \\ B_n J_n(kr) + C_n H_n(kr) & b < r < a \\ D_n J_n(k_o r) & r < b \end{array} \right\} e^{in\varphi} \qquad (3.7)$$

where $k = k_o \sqrt{\mu_r \epsilon_r}$. $J_n$ and $H_n$ represent the Bessel and Hankel functions of first kind and order n, respectively.

The incident plane wave of unit amplitude has the Fourier expansion as

$$U_z^{in} = e^{ik_o x} = e^{ik_o r \cos\varphi} = \sum_{n=-\infty}^{\infty} i^n J_n(k_o r) e^{in\varphi}. \qquad (3.8)$$

The number of unknown coefficients in (3.7) can be reduced by applying boundary conditions that are valid on the closed contours at $r = b$ and at $r = a$

$$B_n = \frac{i^n J_n(k_o a) + H_n(k_o a) A_n}{J_n(ka)\xi_n - H_n(ka)\eta_n} \xi_n \quad , \qquad (3.9)$$

$$C_n = -\frac{i^n J_n(k_o a) + H_n(k_o a) A_n}{J_n(ka)\xi_n - H_n(ka)\eta_n} \eta_n \qquad (3.10)$$

and

$$D_n = \frac{2i}{\pi k_o b \mu_r} \frac{i^n J_n(k_o a) + H_n(k_o a) A_n}{J_n(ka)\xi_n - H_n(ka)\eta_n} \qquad (3.11)$$

where

$$\xi_n = \sqrt{\frac{\epsilon_r}{\mu_r}} H_n'(kb) J_n(k_o b) - H_n(kb) J_n'(k_o b)$$

15

$$\eta_n = \sqrt{\frac{\epsilon_r}{\mu_r}} J'_n(kb)J_n(k_o b) - J_n(kb)J'_n(k_o b)$$

for E-polarized case, and for the other polarization with the corresponding boundary conditions we obtain

$$B_n = \sqrt{\frac{\epsilon_r}{\mu_r}} \frac{i^n J'_n(k_o a) + H'_n(k_o a)A_n}{J'_n(ka)\xi_n - H'_n(ka)\eta_n}\xi_n \quad, \tag{3.12}$$

$$C_n = \sqrt{\frac{\epsilon_r}{\mu_r}} \frac{-i^n J'_n(k_o a) + H'_n(k_o a)A_n}{J'_n(ka)\xi_n - H'_n(ka)\eta_n}\eta_n \tag{3.13}$$

and

$$D_n = \frac{2i}{\pi kb} \frac{i^n J'_n(k_o a) + H'_n(k_o a)A_n}{J'_n(ka)\xi_n - H'_n(ka)\eta_n}\xi_n \tag{3.14}$$

where now,

$$\xi_n = \sqrt{\frac{\mu_r}{\epsilon_r}} H'_n(kb)J_n(k_o b) - H_n(kb)J'_n(k_o b)$$

$$\eta_n = \sqrt{\frac{\mu_r}{\epsilon_r}} J'_n(kb)J_n(k_o b) - J'_n(k_o b)$$

and prime denotes derivative with respect to the argument.

The boundary conditions that are continuity of the magnetic field at the aperture and vanishing electric field on the screen lead to dual series equations for the expansion coefficients

$$\sum_{n=-\infty}^{\infty} x_n \gamma_n e^{in\varphi} = -\sum_{n=-\infty}^{\infty} d_n e^{in\varphi}, \quad |\varphi - \varphi_o| < \theta \tag{3.15}$$

$$\sum_{n=-\infty}^{\infty} x_n e^{in\varphi} = 0, \quad \theta < |\varphi - \varphi_o| \leq \pi \tag{3.16}$$

where

$$x_n = \begin{cases} i^n J_n(k_o a) + H_n(k_o a)A_n \,, & \text{for E-pol} \\ i^n J'_n(k_o a) + H'_n(k_o a)A_n \,, & \text{for H-pol} \end{cases} \tag{3.17}$$

$$d_n = \begin{cases} -\frac{2i^{n+1}}{\pi k_o a H_n(k_o a)} \,, & \text{for E-pol} \\ -\frac{2i^{n+1}}{\pi k_o a H'_n(k_o a)} \,, & \text{for H-pol} \end{cases} \tag{3.18}$$

and

$$\gamma_n = \begin{cases} \frac{H'_n(k_o a)}{H_n(k_o a)} - \sqrt{\frac{\epsilon_r}{\mu_r}} \frac{J'_n(ka)\xi_n - H'_n(ka)\eta_n}{J_n(ka)\xi_n - H_n(ka)\eta_n} \,, & \text{for E-pol} \\ \frac{H_n(k_o a)}{H'_n(k_o a)} - \sqrt{\frac{\epsilon_r}{\mu_r}} \frac{J_n(ka)\xi_n - H_n(ka)\eta_n}{J'_n(ka)\xi_n - H'_n(ka)\eta_n} \,, & \text{for H-pol} . \end{cases} \tag{3.19}$$

## 3.3 Dual-Series-Based Solution

### 3.3.1 E-polarized Plane Wave Incidence

Investigating the asymptotic behavior of $\gamma_n$ as $\mid n \mid \to \infty$, based on the corresponding expressions for cylindrical functions [26], we find

$$\gamma_n \sim -\frac{\mid n \mid}{k_o a}\left(1 + \frac{\beta_n}{\mu_r}\right) \qquad (3.20)$$

where

$$\beta_n = 1 + 2\frac{\mu_r - 1}{\mu_r + 1}\left(\frac{b}{a}\right)^{2n}\left[1 - \frac{\mu_r - 1}{\mu_r + 1}\left(\frac{b}{a}\right)^{2n}\right]^{-1} \qquad (3.21)$$

For $b \neq a$, the dominant term in (3.21) is the first term, which is 1. The remaining terms decrease very fast as n increases. To have a fast convergence of the solution, we add and subtract the asymptotic expression (3.20) from $\gamma_n$ in (3.15), and get the following result

$$\sum_{n=-\infty}^{\infty} x_n \mid n \mid e^{in\varphi} = \sum_{n=-\infty}^{\infty}\left(x_n\Delta_n + \frac{\mu_r k_o a}{\mu_r + 1}d_n\right)e^{in\varphi} ; \qquad \mid \varphi - \varphi_o \mid < \theta \quad (3.22)$$

where

$$\Delta_n = \frac{\mu_r k_o a}{\mu_r + 1}\gamma_n + \mid n \mid \ ,$$

$x_n$ and $d_n$ are given in (3.17) and (3.18), respectively.

Equation (3.22) and (3.16) form canonical dual series equations. This dual series system can be solved by converting into the Riemann-Hilbert problem which is explained in the previous chapter. Assuming that the series (3.16) is term-by-term differentiable, we replace it with the derivative with respect to $\varphi$. The termwise differentiation can be justified as described in [13]. Denoting $\psi = \varphi - \varphi_o$, we have the following equations

$$\sum_{n=-\infty}^{\infty} \tilde{x}_n \mid n \mid e^{in\psi} = F(e^{i\psi}), \qquad \mid \psi \mid < \theta \qquad (3.23a)$$

$$\sum_{n=-\infty}^{\infty} \tilde{x}_n n e^{in\psi} = 0, \qquad \theta < \mid \psi \mid \le \pi \qquad (3.23b)$$

$$\sum_{n=-\infty}^{\infty} (-1)^n \tilde{x}_n = 0 \qquad (3.23c)$$

17

where $\tilde{x}_n = x_n e^{in\varphi_o}$. The last equation is obtained by substituting $\varphi = \pi + \varphi_o$ into (3.16) to account for the elimination of the constant term due to differentiation. The function on the right-hand side of (3.23a) has a Fourier expansion as

$$F(e^{i\psi}) = \sum_{n=-\infty}^{\infty} f_n e^{in\psi} \qquad (3.24)$$

where the coefficients are given as

$$f_n = \left( x_n \Delta_n + \frac{\mu_r k_o a}{\mu_r + 1} d_n \right) e^{in\varphi_o} \quad . \qquad (3.25)$$

By introducing functions $X^{\pm}$ of complex variable $z = |z| e^{i\psi}$ such that

$$X(z) = \begin{cases} X^+(z) = \sum_{n>0} \tilde{x}_n n z^n, & |z| \leq 1 \\ X^-(z) = -\sum_{n<0} \tilde{x}_n n z^n, & |z| \geq 1 \end{cases} \qquad (3.26)$$

and using (3.23a) and (3.23b), the functional equation valid on the whole unit circle $|z| = 1$

$$X^+(e^{i\psi}) + A X^-(e^{i\psi}) = B \qquad (3.27)$$

is obtained with

$$A(\psi) = \begin{cases} +1, & |\psi| < \theta \\ -1, & \theta < |\psi| \leq \pi \end{cases}, \quad B(\psi) = \begin{cases} F(e^{i\psi}), & |\psi| < \theta \\ 0, & \theta < |\psi| \leq \pi \end{cases} .$$

This is the equation which is known to constitute RHP. To arrive at the exact solution of (3.27), it is necessary to restrict the behavior of the unknown function $X(z)$ at the infinity and at the end points of the screen. One may see from (3.23), (3.25) that the frequency dependence is contained only in $F(e^{i\psi})$ term. Assuming that $F(e^{i\psi})$ is known, (3.27) forms a static problem ($k = 0$) for $X(z)$. However, at static limit, the incident plane wave constitutes a superposition of two cross polarized constant fields: electric $E_z$ and magnetic $H_y$. Perfectly conducting cylinder does not perturb axial electric field, but it does perturb transverse magnetic one. So, function $X(z)$ corresponds to the perturbation of $H_y$ by the presence of the screen which then vanishes as $|z| \to \infty$. From (3.5), the field behavior at the edges for $E_z$ and $H_\varphi$, will be like $(|\psi| - \theta)^{1/2}$ and $(|\psi| - \theta)^{-1/2}$, respectively. So, $X(z)$ must have a square root singularity at the edges of the screen.

Further, following the Riemann-Hilbert solution technique described in the previous chapter, we arrive the solution in the form

$$\tilde{x}_m = \sum_{n=-\infty}^{\infty} f_n T_{mn}(\cos\theta) \qquad (3.28)$$

18

where $f_n$ is the Fourier expansion coefficient given in (3.25). $T_{mn}(u)$ is related to the Legendre polynomials ( $P_m$ and $P_n$) and is given in Appendix A.

This form of the solution of the dual series equations is simpler than the one in [12], [16]–[15], since it does not require the separation of equations for $m = 0$ and $m \neq 0$ parts.

By defining

$$\rho_n = A_n / J_n(k_o a) \ ,\qquad\qquad (3.29)$$

one can write (3.28) as

$$\rho_m = \sum_{n=-\infty}^{\infty} K_{mn}\rho_n + S_m, \quad m = 0, \pm 1, \dots \qquad (3.30)$$

where

$$K_{mn} = \frac{H_n(k_o a)J_n(k_o a)}{H_m(k_o a)J_m(k_o a)}\Delta_n W_{mn} \qquad\qquad (3.31)$$

$$S_m = \frac{-i^m}{H_m(k_o a)} + \frac{1}{H_m(k_o a)J_m(k_o a)}\sum_{(n)} i^n \left[ J_n(k_o a)\Delta_n - \frac{2i\mu_r(\mu_r + 1)^{-1}}{\pi H_n(k_o a)} \right] W_{mn}$$

$$(3.32)$$

and

$$W_{mn} = e^{i(n-m)\varphi_o}T_{mn}(\cos\theta) \ . \qquad\qquad (3.33)$$

The coefficients $W_{mn}$ contain all the information about the angular geometry of the screen, as functions of $\theta$ and $\varphi_o$. Expression (3.30) can be written as a single operator equation

$$(I - K)\rho = S \qquad\qquad (3.34)$$

where $\rho = \{\rho_n\}_{n=-\infty}^{\infty}$, $I$ is identity matrix and $K = \{K_{mn}\}_{m,n=-\infty}^{\infty}$. Operator K can be shown (see [13]) to be compact in the Hilbert space of $l_2$ ($\rho \in l_2$ if $\sum_{n=-\infty}^{\infty} |\rho_n|^2 < \infty$). Besides, vector $S = \{S_m\}_{m=-\infty}^{\infty} \in l_2$ as well. It means that (3.34) is a regularized operator equation, and therefore well known Fredholm's theorems are valid [30]: solution $\rho$ does exist and is unique. Moreover, any solution of (3.34) can be shown (see [13]) to satisfy

$$\sum_{n=-\infty}^{\infty} |\rho_n|^2 |n+1| < \infty \qquad\qquad (3.35)$$

as $\rho_n$ decay as $O(n^{-3/2})$ when $|n| \to \infty$. Hence, (3.35) ensures the validity of the edge condition (3.5), [13]. Further, this solution can be approximated with any desired accuracy by means of truncation of the matrix $K = \{K_{mn}\}_{m,n=-\infty}^{\infty}$,

19

and vector $S = \{S_m\}_{m=-\infty}^{\infty}$ for all $|m|, |n| > N_{tr}$. The sequence of approximate solutions is guaranteed to converge to the exact solution for any $k_o a, b/a, \epsilon_r, \mu_r, \theta, \varphi_o$ as $N_{tr} \to \infty$, which is not the general case in the method of moments. In practice, simple numerical rule has been verified. To provide an accuracy of 0.1 %, we had to take $N_{tr} =$ integer part of $(k_o a) + 15$. It is noted that, all the field coefficients in (3.7), namely $A_n$, $B_n$, $C_n$ and $D_n$ are calculated using equations (3.29), (3.9), (3.10) and (3.11), respectively.

We treat the second problem (for outer covering) in a similar way. In (3.7), we replace $a$'s with $b$'s; afterwards the same procedure is followed. The resultant infinite system of linear equations is formally the same as in the previous problem (3.30). It is rewritten below for convenience

$$\rho_m = \sum_{(n)} K_{mn}\rho_n + S_m, \quad m = 0, \pm 1, \dots \tag{3.36}$$

where now

$$K_{mn} = \frac{J_n(k_o a)}{J_m(k_o a)} \frac{H_n(ka)\xi_n - J_n(ka)\eta_n}{H_m(ka)\xi_m - J_m(ka)\eta_m} \Delta_n W_{mn} \tag{3.37}$$

and the coefficients are

$$\xi_n = J_n(kb)H_n'(k_o b) - \sqrt{\frac{\epsilon_r}{\mu_r}} J_n'(kb)H_n(k_o b)$$

$$\eta_n = H_n(kb)H_n'(k_o b) - \sqrt{\frac{\epsilon_r}{\mu_r}} H_n'(kb)H_n(k_o b)$$

and

$$\Delta_n = -\frac{\mu_r k_o a}{\mu_r + 1}\gamma_n + |n| \tag{3.38}$$

where

$$\gamma_n = \frac{J_n'(k_o a)}{J_n(k_o a)} - \sqrt{\frac{\epsilon_r}{\mu_r}} \frac{H_n'(ka)\xi_n - J_n'(ka)\eta_n}{H_n(ka)\xi_n - J_n(ka)\eta_n}$$

Coefficient $S_m$ in (3.36) is now given by

$$S_m = J_m^{-1}(k_o a)[H_m(ka)\xi_m - J_m(ka)\eta_m]^{-1}(-i^m[H_m(ka)s_{2m} - J_m(ka)s_{4m}]$$

$$+ \sum_{(n)} i^n \left\{ [H_n(ka)s_{2n} - J_n(ka)s_{4n}]\Delta_n + 8i\alpha^{-1}[H_n(ka)\xi_n - J_n(ka)\eta_n]^{-1} \right\} W_{mn})$$

$$\tag{3.39}$$

where

$$\alpha = \pi^3 (k_o b)^2 \mu_r (\mu_r + 1)$$

$$s_{2n} = J_n(kb)J_n'(k_o b) - \sqrt{\frac{\epsilon_r}{\mu_r}} J_n'(kb)J_n(k_o b)$$

$$s_{4n} = H_n(kb)J'_n(k_ob) - \sqrt{\frac{\epsilon_r}{\mu_r}}H'_n(kb)J_n(k_ob)$$

The second problem has the same type of operator equation as the previous one.

### 3.3.2  H-polarized Plane Wave Incidence

Investigating the asymptotic behavior of $\gamma_n$ as $\mid n \mid \to \infty$, based on the corresponding expressions for cylindrical functions [26], we find

$$\gamma_n \sim -\frac{k_o a}{\mid n \mid}\left(1 + \frac{\epsilon_r}{\beta_n}\right) \tag{3.40}$$

where

$$\beta_n = 1 + 2\frac{\epsilon_r - 1}{\epsilon_r + 1}\left(\frac{b}{a}\right)^{2n}\left[1 - \frac{\epsilon_r - 1}{\epsilon_r + 1}\left(\frac{b}{a}\right)^{2n}\right]^{-1} \tag{3.41}$$

For $b \neq a$, the dominant term in (3.41) is the first term, which is 1. The remaining terms decrease very fast as n increases. To reduce the problem into canonical dual series equations, we make the following transformation

$$y_n = x_n\gamma_n + d_n \tag{3.42}$$

which leads to the following dual series equations

$$\sum_{(n)} y_n e^{in\varphi} = 0, \qquad\qquad \mid \varphi - \varphi_o \mid < \theta \tag{3.43}$$

$$\sum_{(n)} y_n\tilde{\gamma}_n e^{in\varphi} = -\sum_{(n)} d_n\tilde{\gamma}_n e^{in\varphi}, \qquad \theta <\mid \varphi - \varphi_o \mid\leq \pi \tag{3.44}$$

where $\tilde{\gamma}_n$ is equal to $1/\gamma_n$ and its large index behavior is given as

$$\tilde{\gamma}_n \sim -\frac{\mid n \mid}{k_o a}\left(\frac{1}{\epsilon_r + 1}\right) \quad . \tag{3.45}$$

Adding and subtracting the asymptotic expression (3.45) from $\tilde{\gamma}_n$ in (3.44), we get the following result

$$\sum_{(n)} y_n \mid n \mid e^{in\varphi} = \sum_{(n)} [y_n\Delta_n + (\mid n \mid -\Delta_n)d_n]\, e^{in\varphi} \quad \theta <\mid \varphi - \varphi_o \mid\leq \pi \tag{3.46}$$

where

$$\Delta_n = k_o a(\epsilon_r + 1)\tilde{\gamma}_n + \mid n \mid \, , \tag{3.47}$$

21

$y_n$ and $d_n$ are given in (3.42) and (3.18), respectively.

Equation (3.46) and (3.43) form canonical dual series equations. This dual series system can be solved by converting the problem into Riemann-Hilbert problem [13], [16], described in the previous chapter. Assuming that the series (3.43) is term-by-term differentiable, we replace it with the derivative with respect to $\varphi$. Denoting $\psi = \varphi - \varphi_o + \pi$ and $\alpha = \pi - \theta$, we have the following equations

$$\sum_{(n)} \tilde{y}_n \mid n \mid e^{in\psi} = F(e^{i\psi}), \qquad \mid \psi \mid < \alpha$$

$$\sum_{(n)} \tilde{y}_n n e^{in\psi} = 0, \qquad \alpha < \mid \psi \mid \leq \pi \qquad (3.48)$$

$$\sum_{(n)} \tilde{y}_n = 0$$

where $\tilde{y}_n = y_n(-1)^n e^{in\varphi_o}$. The last equation is obtained by substituting $\varphi = \pi + \varphi_o$ into (3.43) to account for the elimination of the constant term due to differentiation. The free-term function on the right-hand side of (3.48) has a Fourier expansion as

$$F(e^{i\psi}) = \sum_{(n)} f_n e^{in\psi} \qquad (3.49)$$

where the coefficients are given as

$$f_n = (-1)^n \left[ y_n \Delta_n + d_n(\mid n \mid - \Delta_n) \right] e^{in\varphi_o} . \qquad (3.50)$$

By introducing functions $X^{\mp}$ of complex variable $z = \mid z \mid e^{i\psi}$ such that

$$X(z) = \begin{cases} X^+(z) = \sum_{n>0} \tilde{y}_n n z^n, & |z| \leq 1 \\ X^-(z) = -\sum_{n<0} \tilde{y}_n n z^n, & |z| \geq 1 \end{cases} \qquad (3.51)$$

we transform the first two equations of (3.48) to functional equation valid on the whole unit circle $\mid z \mid = 1$

$$X^+(e^{i\psi}) + A X^-(e^{i\psi}) = B \qquad (3.52)$$

with

$$A(\psi) = \begin{cases} +1, & \mid \psi \mid < \alpha \\ -1, & \alpha < \mid \psi \mid \leq \pi \end{cases} , \quad B(\psi) = \begin{cases} F(e^{i\psi}), & \mid \psi \mid < \alpha \\ 0, & \alpha < \mid \psi \mid \leq \pi . \end{cases}$$

The exact solution of (3.52) is given by the RHP solution subject to necessary restrictions, that is the behavior of the unknown function $X(z)$ at infinity

and at the end points of the screen. In this problem, function $X(z)$ corresponds to the perturbation of static electric field by the presence of the screen. That is why it is clear that $X(z)$ vanishes as $|z| \to \infty$, and has a square root singularity at the edges of the screen. The field behavior at the edges, from Meixner edge condition, for $E_\varphi$ and $H_z$, will be like $(|\psi| - \theta)^{-1/2}$ and $(|\psi| - \theta)^{1/2}$, respectively.

Hence the solution is obtained as

$$\tilde{y}_m = \sum_{(n)} f_n T_{mn}(-\cos\theta) \tag{3.53}$$

where $f_n$ is the Fourier expansion coefficient given in (3.50). $T_{mn}$ is related to Legendre polynomials, and is given in Appendix A. By defining

$$\mu_n = A_n / J_n'(k_o a) , \tag{3.54}$$

one can write (3.53) as

$$\mu_m = \sum_{(n)} K_{mn}\mu_n + S_m, \quad m = 0. \pm 1, \ldots \tag{3.55}$$

where

$$K_{mn} = \frac{H_n'(k_o a)J_n'(k_o a)}{H_m'(k_o a)J_m'(k_o a)} \frac{\gamma_n}{\gamma_m} \Delta_n W_{mn} \tag{3.56}$$

$$S_m = \frac{-i^m}{H_m'(k_o a)} - \frac{2i^{m+1}(\pi k_o a)^{-1}}{J_m'(k_o a)[H_m'(k_o a)]^2 \gamma_n}$$

$$+ \frac{1}{H_m'(k_o a)J_m'(k_o a)\gamma_n} \sum_{(n)} i^n \left[ J_n'(k_o a)\gamma_n\Delta_n + \frac{2i}{\pi k_o a H_n'(k_o a)} \right] W_{mn} \tag{3.57}$$

and

$$W_{mn} = e^{i(n-m)\varphi_o}(-1)^{m+n}T_{mn}(-\cos\theta) . \tag{3.58}$$

The coefficients $W_{mn}$ contain all the information about the angular geometry of the screen.

Expression (3.55) can be written as a single operator equation

$$(I - K)\mu = S \tag{3.59}$$

Similar to E-pol. case, one can show that (3.59) is a regularized operator equation which satisfies the well known Fredholm's theorems: solution $\mu$ does

exist and is unique. Moreover, any solution of (3.59) can be shown to satisfy

$$\sum_{(n)} |\mu_n|^2 |n+1| < \infty \tag{3.60}$$

Hence, (3.60) ensures the validity of the edge condition (3.5). Finally, this solution can be approximated with any desired accuracy by means of truncation of the matrix $K = \{K_{mn}\}_{m,n=-\infty}^{\infty}$, and vector $S = \{S_m\}_{m=-\infty}^{\infty}$ for all $|m|, |n| > N_{tr}$. The sequence of approximate solutions is guaranteed to converge to exact solution for any $k_o a, b/a, \epsilon_r, \mu_r, \theta, \varphi_o$ as $N_{tr} \to \infty$, which is not the general case in the method of moments. The field coefficients in (3.7), namely, $A_n$, $B_n$, $C_n$, and $D_n$ are calculated by using equations (3.54), (3.12), (3.13) and (3.14), respectively.

The outer covering case is also treated in a similar way. In (3.7), we replace a's with b's; afterwards the same procedure is followed. The resultant infinite system of linear equations is formally the same as in the previous problem (3.55)

$$\mu_m = \sum_{(n)} K_{mn}\mu_n + S_m, \quad m = 0, \pm 1, \ldots \tag{3.61}$$

where now

$$K_{mn} = \frac{J_n'(k_o a)}{J_m'(k_o a)} \frac{H_n'(ka)\xi_n - J_n'(ka)\eta_n}{H_m'(ka)\xi_m - J_m'(ka)\eta_m} \frac{\gamma_n}{\gamma_m} \Delta_n W_{mn} \tag{3.62}$$

and the coefficients are

$$\xi_n = J_n(kb)H_n'(k_o b) - \sqrt{\frac{\mu_r}{\epsilon_r}} J_n'(kb) H_n(k_o b)$$

$$\eta_n = H_n(kb)H_n'(k_o b) - \sqrt{\frac{\mu_r}{\epsilon_r}} H_n'(kb) H_n(k_o b)$$

and

$$\Delta_n = |n| - \frac{k_o a(1 + \epsilon_r)}{\gamma_n} \tag{3.63}$$

where

$$\gamma_n = \frac{J_n(k_o a)}{J_n'(k_o a)} - \sqrt{\frac{\epsilon_r}{\mu_r}} \frac{H_n(ka)\xi_n - J_n(ka)\eta_n}{H_n'(ka)\xi_n - J_n'(ka)\eta_n}$$

Coefficient $S_m$ in (3.61) is now given by

$$S_m = \frac{-i^m [H_m'(ka)s_{2m} - J_m'(ka)s_{4m}] + 8i\alpha^{-1}[H_m'(ka)\xi_m - J_m'(ka)\eta_m]^{-1}\gamma_m^{-1}}{J_m'(k_o a)[H_m'(ka)\xi_m - J_m'(ka)\eta_m]}$$

24

$$+ \frac{\sum\limits_{(n)} i^n \left\{ [H'_n(ka)s_{2n} - J'_n(ka)s_{4n}]\Delta_n\gamma_n + 8i\alpha^{-1}[H'_n(ka)\xi_n - J'_n(ka)\eta_n]^{-1} \right\} W_{mn}}{J'_m(k_oa)[H'_m(ka)\xi_m - J'_m(ka)\eta_m]\gamma_m}$$

$$(3.64)$$

where

$$\alpha = \pi^3 (k_o a)(k_o b)^2 \mu_r \epsilon_r$$

$$s_{2n} = J_n(kb)J'_n(k_ob) - \sqrt{\frac{\mu_r}{\epsilon_r}} J'_n(kb)J_n(k_ob)$$

$$s_{4n} = H_n(kb)J'_n(k_ob) - \sqrt{\frac{\mu_r}{\epsilon_r}} H'_n(kb)J_n(k_ob)$$

The second problem has the same type of operator equation as the previous one.

# Chapter 4

# NUMERICAL RESULTS and DISCUSSION

In this chapter numerical results are obtained for the radar cross section (RCS) behavior of a CBA which is coated either from inside or from outside with absorbing materials. The associated formula for RCS for E-pol incidence is given as

$$\sigma_{bs} = \lim_{r \to \infty} 2\pi r \frac{\mid E^{sc}(r,\pi) \mid^2}{\mid E^{in} \mid^2} \quad ,$$

which can be written in terms of expansion coefficients as

$$\sigma_{bs} = \frac{4}{k_o} \left| \sum_{-N_{tr}}^{N_{tr}} \rho_n i^n J_n(k_o a) \right|^2$$

We have normalized RCS with respect to $\pi a$ which is the geometrical optics value for the perfectly conducting closed circular cylinder. The normalized RCS results are presented with respect to frequency, aspect angle of the screen, thickness of the absorbing layer and different aperture sizes for both polarizations.

If otherwise not stated, $\theta$ is taken as $30°$ (aperture size of $60°$), and the materials used for coating are shellac, natural XL ($\epsilon_r = 3.45 + 0.25i$, $\mu_r = 1$) [28] (dashed curves) and poly-2.5-dichlorostyrene ($\epsilon_r = 7.3$, $\mu_r = 0.91 + 0.32i$) [5] (solid curves). The thickness of the absorbing layer is 10% of the radius of the screen. For comparison, dotted curves represent the RCS calculated for the same CBA without any coating.

# 4.1 Radar Cross Section versus Frequency

## 4.1.1 E-Polarized Case

The normalized RCS results are presented in Figures 4.1 to 4.6 as a function of frequency for different coating materials and different orientations of the aperture.

It is noted that for $\varphi_o = 180^o$ case, the average level of RCS of uncoated CBA is much higher than that of closed uncoated circular cylinder of the same radius (dash-dotted curve in Figure 4.2). In addition, strong resonances are observed in the RCS. The resonances are due to the excitation of the damped natural modes of the screen as a cavity-backed aperture. The damped modes originate from the eigenmodes of the closed cylinder, $E_{mn}$, being shifted in frequency and splitted into even/odd pairs, $E_{mn}^{\pm}$ due to cutting of the slot.

The shifted frequency locations have been calculated previously [14] for uncoated CBA. Iterative-perturbation analysis of the characteristic equation $det(I - K) = 0$, under assumption that $\tau = \sin(\theta/2) \to 0$, had been carried out due to the strongly-diagonal shape of the matrix. The natural frequencies are complex-valued with real parts smaller than the corresponding zeros of the Bessel functions. They are found as asymptotic series

$$k_{mn}^{+}a = \nu_{mn} - \frac{\delta_m}{2}\nu_{mn}\tau^2 \left[ 1 + \left( \frac{1}{2} - m^2 + i\zeta_{mn} \right) \tau^2 \right] + O(\tau^6), \qquad (4.1)$$

for the even modes ($m = 0, 1, 2, ...$), and

$$k_{mn}^{-}a = \nu_{mn} - \frac{1}{2}m^2\nu_{mn}\tau^4 \left( 1 + i\Upsilon_{mn}\tau^4 \right) + O(\tau^{10}) \qquad (4.2)$$

for the odd modes ($m = 1, 2, ...$) of the empty circular slitted cavity. In (4.1) and (4.2),

$$\zeta_{mn} = \pi^{-1} \sum_{s=0,\neq m}^{\infty} \delta_s |H_s(\nu_{mn})|^{-2}, \qquad \Upsilon_{mn} = \pi^{-1} \sum_{s=1,\neq m}^{\infty} s^2 |H_s(\nu_{mn})|^{-2} \qquad (4.3)$$

and $\delta_o = 1, \delta_s = 2$ for $s \neq 0$, and $\nu_{mn}$ is the n-th zero of $J_m(x)$.

The shifted frequency locations show good agreement with the minima of RCS in the numerical results for uncoated CBA at $\varphi_o = 180^o$. Note that, for the symmetrical position of the slitted cylinder, i.e. when $\varphi_o = 0^o$ or $180^o$,

Figure 4.1: The normalized RCS of an uncoated and outer-coated CBA for E-pol. incidence for two different absorbing materials with CBA having $60°$ aperture size, $\varphi_o = 180°$ and the coating radius b=1.1a; solid line: $\epsilon_r = 7.3$, $\mu_r = 0.91 + 0.32i$; dashed line: $\epsilon_r = 3.45 + 0.25i$, $\mu_r = 1$; dotted line: uncoated cylinder, i.e. $\epsilon_r = 1$, $\mu_r = 1$.

there may exist only even modes, i.e. $E_{mn}^+$'s, however for unsymmetrical cases both resonances, even and odd modes, i.e $E_{mn}^+$ and $E_{mn}^-$ do appear. The excited modes corresponding to the first four resonance frequencies for $\varphi_o = 180°$ case are known as $E_{01}^+, E_{11}^+, E_{21}^+, E_{02}^+$, [17].

The effect of the presence of the absorbing material on the outer and inner wall of CBA are demonstrated in Figures 4.1 and 4.2, respectively for the case of aperture in the illumination region. As observed in these figures, the lowest order peak cannot be reduced by using absorbing dielectric material. However when the frequency increases, the resonance peaks are reduced. It is due to the fact that low frequency E-field has zero value on the screen and has a maximum on the axis of the cylinder, as zeroth harmonic is dominating. But when the frequency is increased, the number of azimuthal harmonics of

Figure 4.2: The normalized RCS of an unslitted cylinder, uncoated and inner-coated CBA for E-pol incidence for two different absorbing materials with CBA having $60°$ aperture size, $\varphi_o = 180°$ and the coating radius b=0.9a; solid line: $\epsilon_r = 7.3$, $\mu_r = 0.91 + 0.32i$; dashed line: $\epsilon_r = 3.45 + 0.25i$, $\mu_r = 1$; dotted line: uncoated cylinder, i.e. $\epsilon_r = 1$, $\mu_r = 1$; dot-dashed line: unslitted cylinder.

comparable amplitude also increases and the location of the maximum of E-field moves away from the axis. Therefore, resonances of higher order modes can be suppressed by coating the screen with the absorbing material from inside. To reduce the lowest order resonance peak, one needs to use magnetic absorbing material as seen in Figures 4.1 and 4.2. Since the magnetic field has an azimuthal component, which is not zero on the screen, it can be suppressed by using lossy magnetic material which results in a lower back scattered power. Coating from outside has no effect on the internal resonances but it helps only to decrease the amplitude of the incident field entering into cavity. Therefore, the sharp minima cannot be suppressed, but the average level of RCS is reduced as seen in Figure 4.1. So the resonances are still sharp which may cause the target to be easily identified.
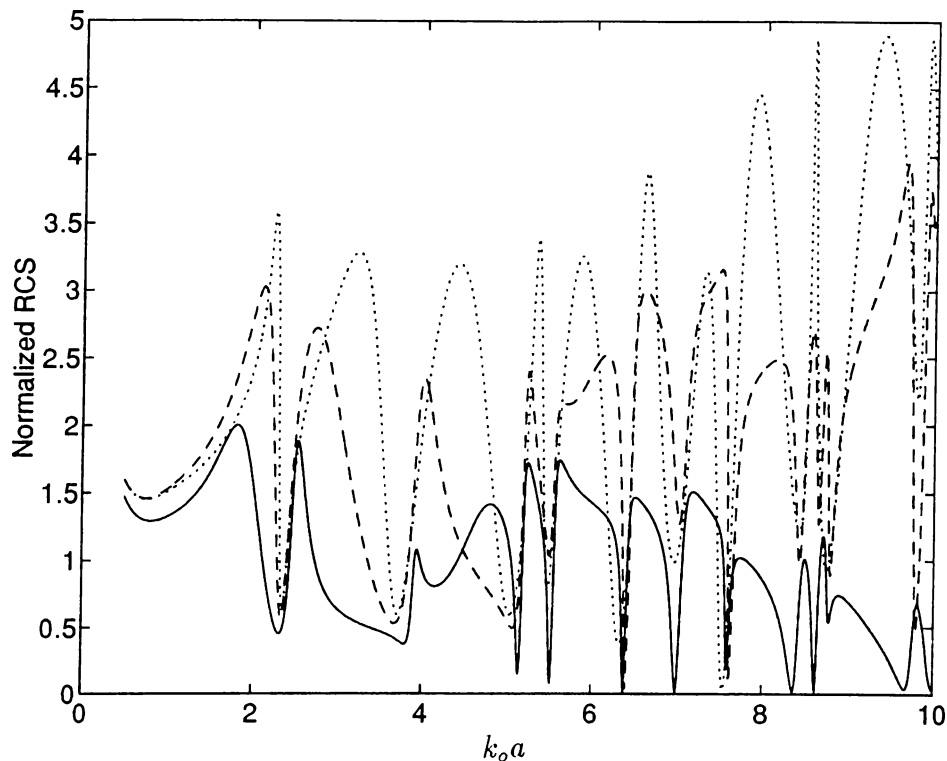
Figure 4.3: The normalized RCS of an uncoated and outer-coated CBA for E-pol. incidence for two different absorbing materials with CBA having $60°$ aperture size, $\varphi_o = 90°$ and the coating radius b=1.1a; solid line: $\epsilon_r = 7.3$, $\mu_r = 0.91 + 0.32i$; dashed line: $\epsilon_r = 3.45 + 0.25i$, $\mu_r = 1$; dotted line: uncoated cylinder, i.e. $\epsilon_r = 1$, $\mu_r = 1$.

As an example of nonsymmetrical excitation, we examine the case of $90°$ orientation, i.e. when the aperture is looking up. Coating from outside is much effective for reducing the average level of the RCS, but there are still sharp resonances (See Figure 4.3). If the coating is from outside, some of the energy is absorbed by the coating material. So, the amplitudes of the resonance peaks are reduced. On the other hand, as seen in Figure 4.4, coating from inside is again effective for suppressing the resonances, except the lowest one. The resonance phenomena are greatly reduced if the frequency is increased and magnetic coating is used.

In Figures 4.5 and 4.6, the results are obtained for the case when the aperture is in the shadow region. Coating from outside is more effective as seen in Figure 4.5. There is no effect of coating from inside, simply because there are almost no resonances in RCS as seen in Figure 4.6. The results are very

30
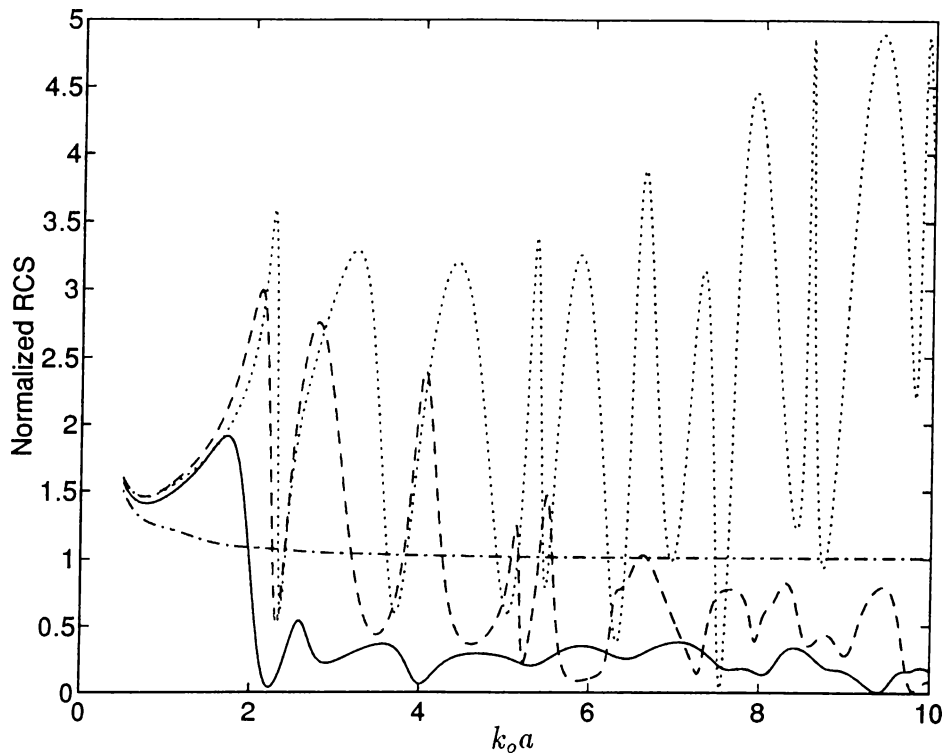
Figure 4.4: The normalized RCS of an uncoated and inner-coated CBA for E-pol. incidence for two different absorbing materials with CBA having $60°$ aperture size, $\varphi_o = 90°$ and the coating radius b=0.9a; solid line: $\epsilon_r = 7.3$, $\mu_r = 0.91 + 0.32i$; dashed line: $\epsilon_r = 3.45 + 0.25i$, $\mu_r = 1$; dotted line: uncoated cylinder, i.e. $\epsilon_r = 1$, $\mu_r = 1$.
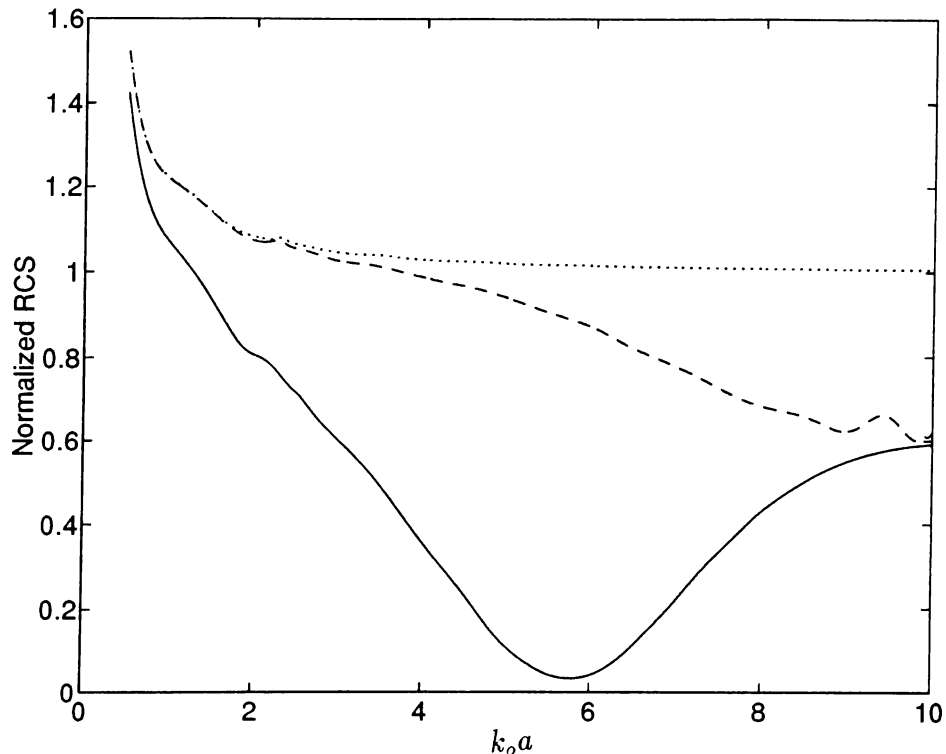
Figure 4.5: The normalized RCS of an uncoated and outer-coated CBA for E-pol incidence for two different absorbing materials with CBA having $60°$ aperture size, $\varphi_o = 0°$ and the coating radius b=1.1a; solid line: $\epsilon_r = 7.3$, $\mu_r = 0.91 + 0.32i$; dashed line: $\epsilon_r = 3.45 + 0.25i$, $\mu_r = 1$; dotted line: uncoated cylinder, i.e. $\epsilon_r = 1$, $\mu_r = 1$.

similar to the closed cylinder case (see Figure 4.2, dash-dotted curve). This happens because the E-polarized excitation induces only longitudinal current on a cylindrical scatterer, hardly reaching the shadow part of surface, and hence, not exciting the interior of CBA. It is also noted that the solid curve in Figure 4.5 is similar to the one in Figure 4.3. The frequency value at which RCS has a broad minimum in those figures corresponds to the frequency at which the reflection coefficient is minimum for quarter-wavelength magneto-dielectric coating on a perfectly conducting plane.
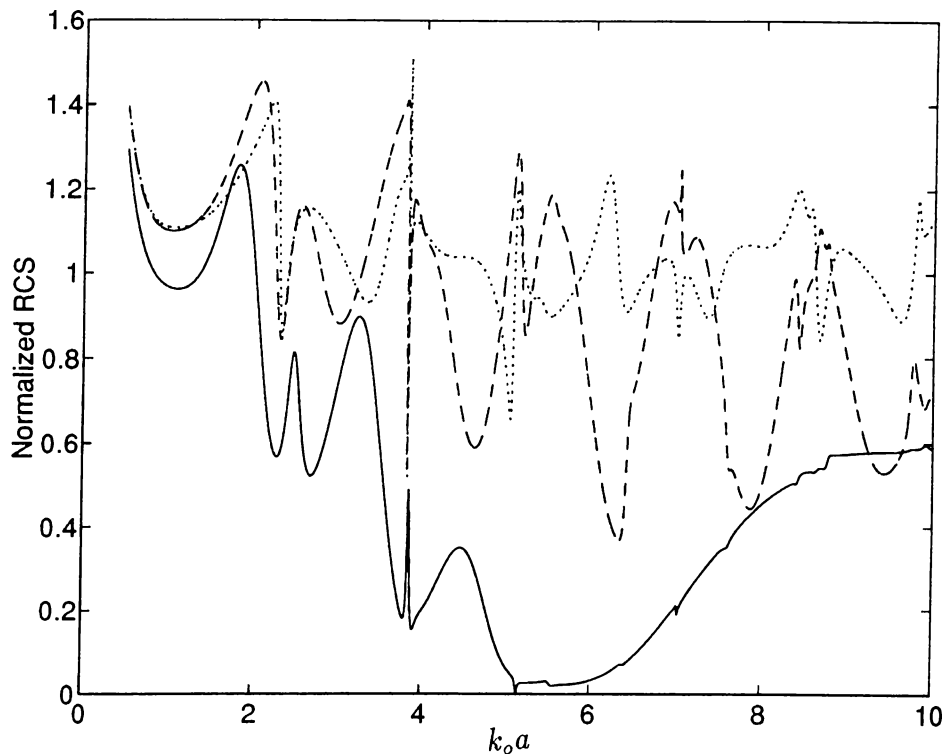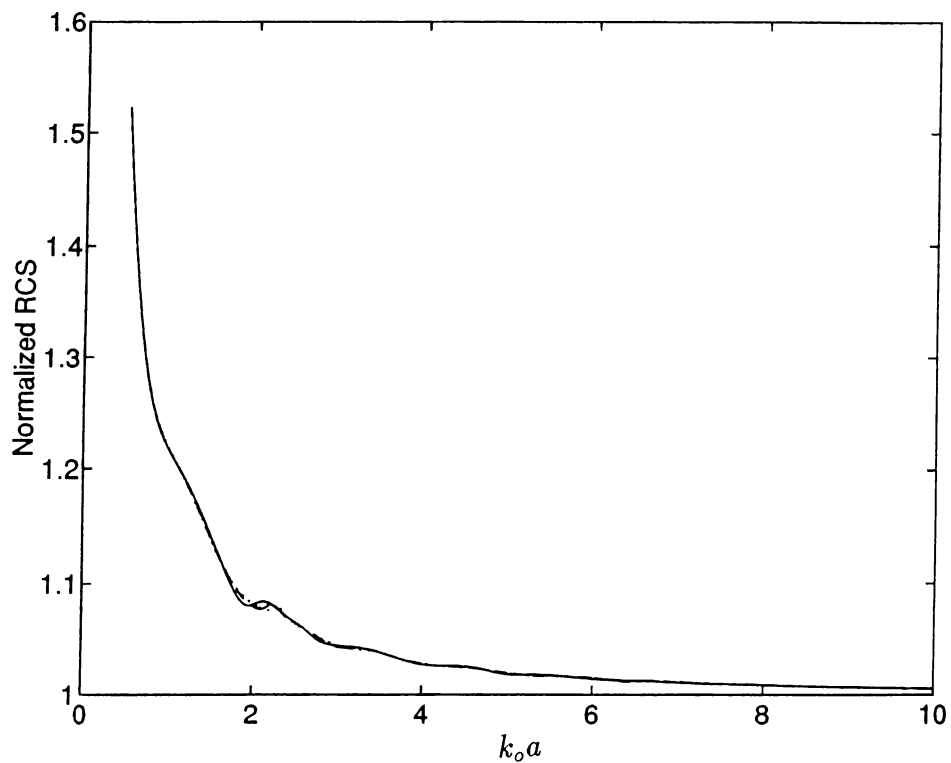
Figure 4.6: The normalized RCS of an uncoated and inner-coated CBA for E-pol incidence for two different absorbing materials with CBA having $60°$ aperture size, $\varphi_o = 0°$ and the coating radius b=0.9a; solid line: $\epsilon_r = 7.3$, $\mu_r = 0.91 + 0.32i$; dashed line: $\epsilon_r = 3.45 + 0.25i$, $\mu_r = 1$; dotted line: uncoated cylinder, i.e. $\epsilon_r = 1$, $\mu_r = 1$.
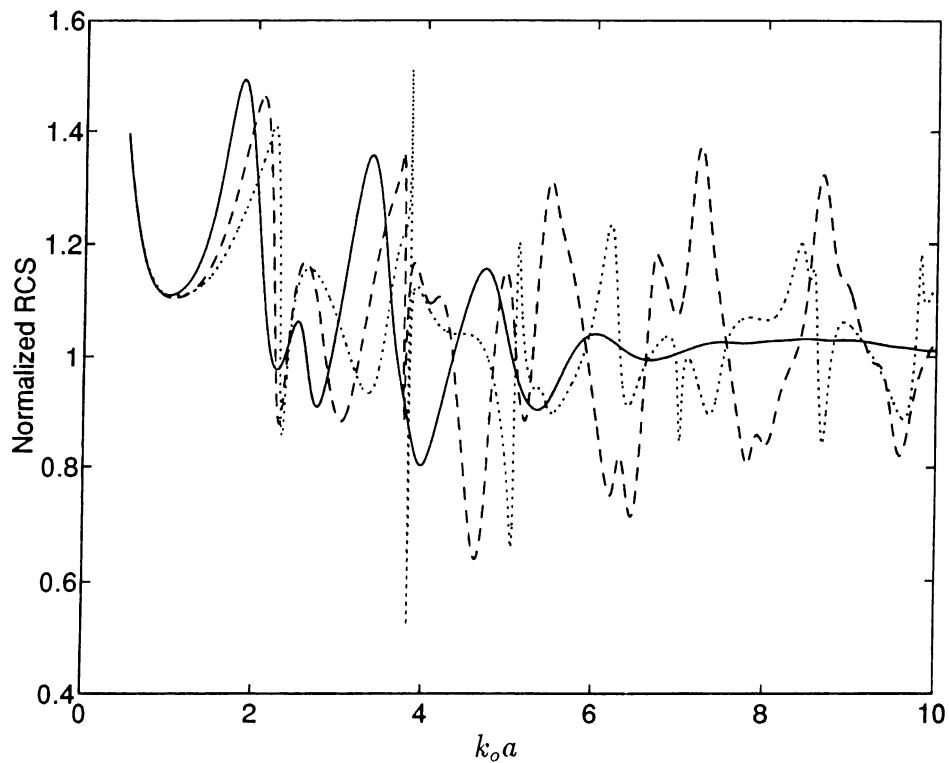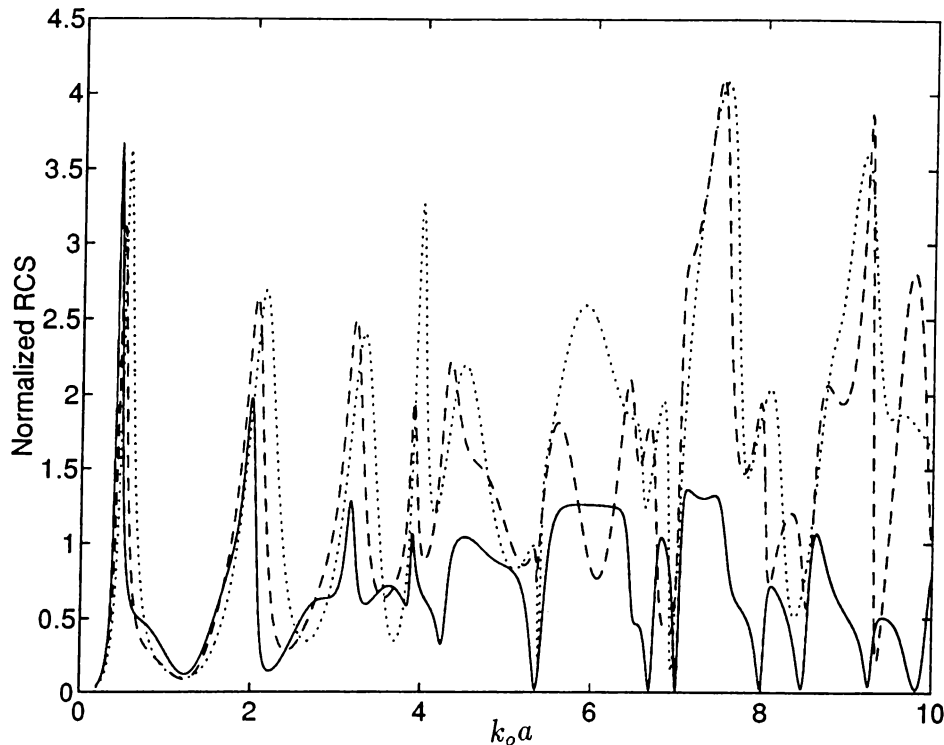
Figure 4.7: The normalized RCS of an uncoated and outer-coated CBA for H-pol. incidence for two different absorbing materials with CBA having 60° aperture size, $\varphi_o = 180°$ and the coating radius b=1.1a; solid line: $\epsilon_r = 7.3$, $\mu_r = 0.91 + 0.32i$; dashed line: $\epsilon_r = 3.45 + 0.25i$, $\mu_r = 1$; dotted line: uncoated cylinder, i.e. $\epsilon_r = 1$, $\mu_r = 1$.

## 4.1.2 H-polarized Case

Unlike the E-polarized case, there appears a low frequency spike in the RCS which does not correspond to any interior resonance of the closed cavity (see Figures 4.7 and 4.8). From mathematical point of view, the low frequency resonance has a singular nature. Any interior Neumann boundary-value problem is known to have the zero as the lowest eigenvalue with arbitrary constant as eigen function. However, in electromagnetics this constant can be shown to be identically equal to zero. The effect of cutting the slot is to shift this zero frequency by a small complex number

$$k_{oo}a \approx (-2\ln(\sin\frac{\theta}{2}))^{-1/2}(1 + \frac{i\pi}{16}\ln^{-1}(\sin\frac{\theta}{2})) . \qquad (4.4)$$

The other effect is that the corresponding (generalized) eigenfunction is no more an identical zero with E-field taking maximum values in the vicinity of

34

the slot.

As it was pointed out in [19], this low frequency resonance is of the same nature as so-called Helmholtz mode of oscillations in acoustic cavities investigated by Rayleigh [33].

The contour plots of the electric field lines (parallel to $H_z$ =const lines) are given in [17], [19]. It is observed that the electric field is concentrated in the aperture region of the cylinder whereas the magnetic field is maximum in its interior which resembles the acoustic Helmholtz resonator in which the kinetic energy of the acoustic oscillations is maximum at the aperture and the potential energy of the compression is maximum in the cavity. Hence, the concentration of electric and magnetic fields in different bounded regions makes it possible to regard the slitted cylinder as a high Q circuit with lumped parameters. The edges of the slit play the role of capacitance, while the walls of the cylinder play the role of inductance. Since the wavelength is much larger than any linear dimension, one may use static methods to find out capacitance and inductance values as [14]

$$L \approx \frac{4\pi}{c}a^2, \quad C \approx \frac{1}{2\pi c}\log\frac{2}{\theta},$$

where $c$ is the speed of light, then the resonant frequency is

$$k_o = \left[\frac{1}{2}\log^{-1}\frac{2}{\theta}\right]^{1/2} \tag{4.5}$$

which is the real part of (4.4). The location of the low frequency resonance is correctly determined in [14] via finding the root of the characteristic equation, and by using equivalent ring resonator approach in [8]. Helmholtz resonance is of special interest as its eigen frequency in (4.4) tends to zero as $\theta \to 0$. At the resonant frequency, $k'_{oo} = Re(k_{oo})$,

$$\sigma_{bs} = \frac{4}{k'_{oo}} + O(k'_{oo}a^2)$$

for a slitted cylinder [13],[14]. So, the resonant value tends to infinity as $\theta \to 0$, in contrast with so-called Rayleigh rule for low frequency scattering from smooth cylinders which is $\sigma_{bs} = O(k^3 a^4)$.

The shifted frequency locations have been calculated previously [14] for uncoated CBA. Iterative-perturbation analysis of the characteristic equation $det(I - K) = 0$, under assumption that $\tau = \sin(\theta/2) \to 0$, had been carried out due to quasi-diagonal shape of the matrix. The natural frequencies

are complex-valued with real parts higher than corresponding zeros of Bessel functions. They are found as asymptotic series

$$k^+_{mn}a \approx \nu_{mn} + \nu_{mn}\left[\delta_m(\nu^2_{mn} - m^2)ln\tau\right]^{-1}(1 + i\zeta_{mn}ln^{-1}\tau), \qquad (4.6)$$

for the even modes $(m = 1, 2, ...)$, and

$$k^-_{mn}a \approx \nu_{mn} + \nu_{mn}m^2(\nu^2_{mn} - m^2)^{-1}\tau^2(1 - 2i\Upsilon_{mn}\tau^2) \qquad (4.7)$$

for the odd modes $(m = 1, 2, ...)$ of the empty circular slitted cavity. In (4.6) and (4.7),

$$\zeta_{mn} = \pi^{-1}\nu^{-2}_{mn}\sum_{s=\neq 0,m}^{\infty}|H'_s(\nu_{mn})|^{-2}, \qquad \Upsilon_{mn} = \pi^{-1}\nu^{-2}_{mn}\sum_{s=1,\neq m}^{\infty}s^2|H'_s(\nu_{mn})|^{-2}$$

$$(4.8)$$

and $\delta_o = 1, \delta_s = 2$ for $s \neq 0$, and $\nu_{mn}$ is the n-th zero of $J'_m(x)$. The details of this solution technique is given in the Appendix B for completeness.

The shifted frequency locations show good agreement with the maxima of RCS in the numerical results for uncoated CBA at $\varphi_o = 180°$. Note that, for the symmetrical position of the slitted cylinder, i.e. when $\varphi_o = 0°$ or $180°$, there may exist only even modes, i.e. $H^+_{mn}$'s, however for unsymmetrical cases both resonances, even and odd modes, i.e $H^+_{mn}$ and $H^-_{mn}$ do appear in closely spaced pair. All the peaks of RCS are of finite amplitude. This is because the perturbed eigen-frequencies are now complex numbers with negative imaginary parts, see (4.4), (4.6) and (4.7). The quality factor of odd modes are much higher than even modes since the imaginary part of $k^-_{mn}$ is less than of $k^+_{mn}$ [14]. The excited modes corresponding to the first four resonance frequencies for $\varphi_o = 180°$ case are known as $H^+_{11}, H^+_{21}, H^+_{01}, H^+_{31}$. Contrary to E-polarized case, all the resonances are slightly higher than the corresponding closed cavity resonances. This is due to the difference in the direction of the induced current which flows circumferentially in the H-polarization whereas axially in E-polarized case. Also, it is noted that the quality factor of the resonance spikes in RCS spectrum is much larger in E-polarized case than H-pol. case (see Figures 4.1 and 4.7). Since the current flows in the circumferential direction in H-pol. case, it causes a much more loss of energy than E-pol case.

Figure 4.7 and 4.8 illustrate the effect of the presence of the absorbing material on the outer and inner wall of CBA, respectively, for the case of aperture in the illuminated region. As observed in these figures, when the frequency increases, the resonance peaks are reduced. It is due to the fact that when
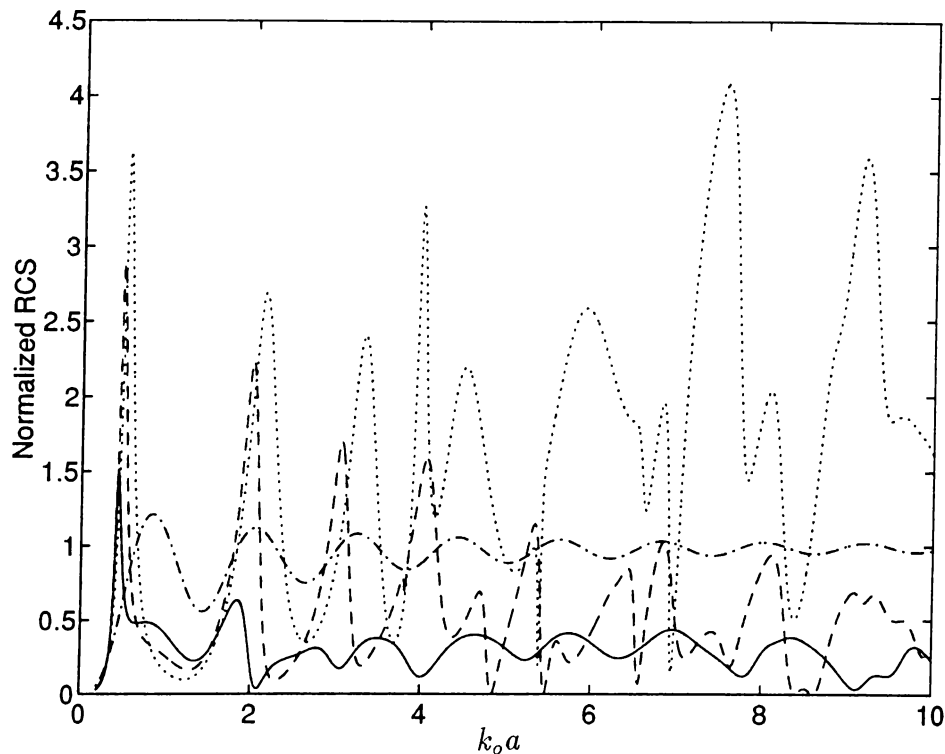
Figure 4.8: The normalized RCS of an unslitted, uncoated and inner-coated CBA for H-pol. incidence for two different absorbing materials with CBA having 60° aperture size, $\varphi_o = 180°$ and the coating radius b=0.9a; solid line: $\epsilon_r = 7.3$, $\mu_r = 0.91 + 0.32i$; dashed line: $\epsilon_r = 3.45 + 0.25i$, $\mu_r = 1$; dotted line: uncoated cylinder, i.e. $\epsilon_r = 1$, $\mu_r = 1$, dot-dashed line: unslitted cylinder.

the frequency is increased, the resonance field is concentrated near the walls of the cavity. Therefore, resonances of higher order modes can be suppressed by coating the screen with the absorbing material from inside. Coating from outside has no effect on the Q-factor of the internal resonances as in the case of E-pol. incidence (see Figure 4.7).

For 90° orientation of the screen, as in the case of E-pol incidence, coating from outside is again effective for reducing the average level of RCS, but there are still sharp resonances (see Figure 4.9), on the other hand coating from inside is again effective for suppressing the resonances. As the frequency increases, the resonance phenomena are greatly reduced and RCS approaches to the geometric optics value as seen in Figure 4.10.

In Figures 4.11 and 4.12, similar results are obtained for the case when the

Figure 4.9: The normalized RCS of an uncoated and outer-coated CBA for H-pol. incidence for two different absorbing materials with CBA having 60° aperture size, $\varphi_o = 90°$ and the coating radius b=1.1a; solid line: $\epsilon_r = 7.3$, $\mu_r = 0.91 + 0.32i$; dashed line: $\epsilon_r = 3.45 + 0.25i$, $\mu_r = 1$; dotted line: uncoated cylinder, i.e. $\epsilon_r = 1$, $\mu_r = 1$.

aperture is in the shadow region. Contrary to E-polarized case, the results are different from the closed cylinder case (See Figure 4.2, dash-dotted curve). This happens because the E-polarized excitation induces only longitudinal current on a cylindrical scatterer, hardly reaching the shadow part of surface, and hence, not exciting the interior of CBA, whereas, H-polarized excitation induces current in the circumferential direction. Therefore, the presence of aperture causes a much stronger response than E-polarized case. At lower frequencies there is no actual shadow zone on the surface of the CBA. That's why, the resonances are equally effective for any aspect angle of the aperture. It is noted that the solid curve in Figure 4.11 is similar to the one in Figure 4.9. The frequency value at which RCS has a broad minimum in those figures corresponds to the frequency at which the reflection coefficient is minimum for magneto-dielectric coating on a perfectly conducting plane.

Figure 4.10: The normalized RCS of an uncoated and inner-coated CBA for H-pol. incidence for two different absorbing materials with CBA having $60°$ aperture size, $\varphi_o = 90°$ and the coating radius b=0.9a; solid line: $\epsilon_r = 7.3$, $\mu_r = 0.91 + 0.32i$; dashed line: $\epsilon_r = 3.45 + 0.25i$, $\mu_r = 1$; dotted line: uncoated cylinder, i.e. $\epsilon_r = 1$, $\mu_r = 1$.
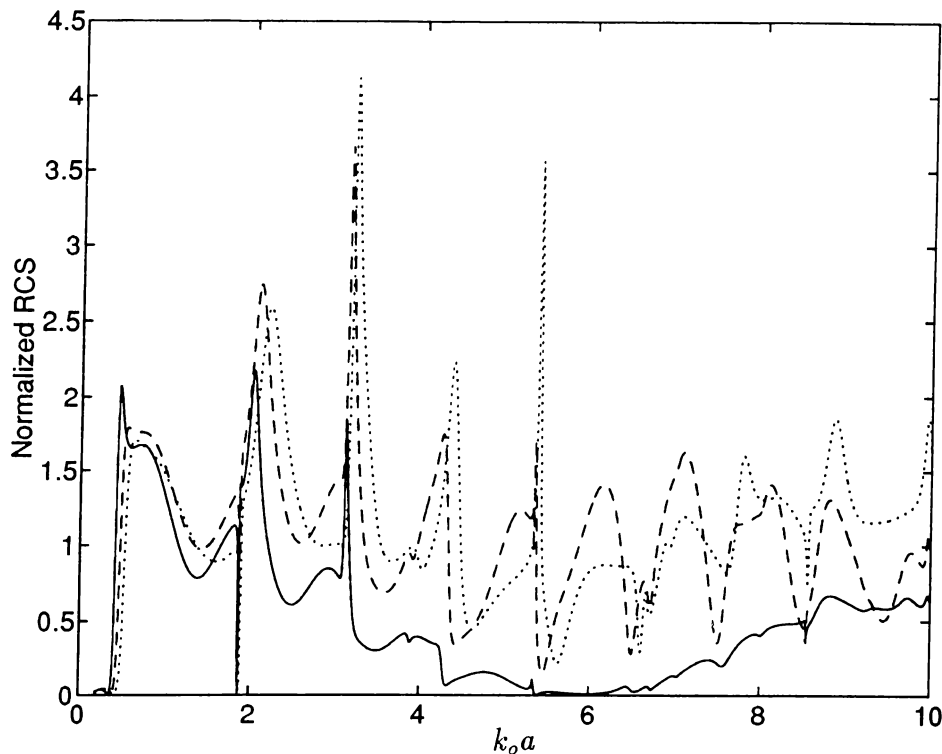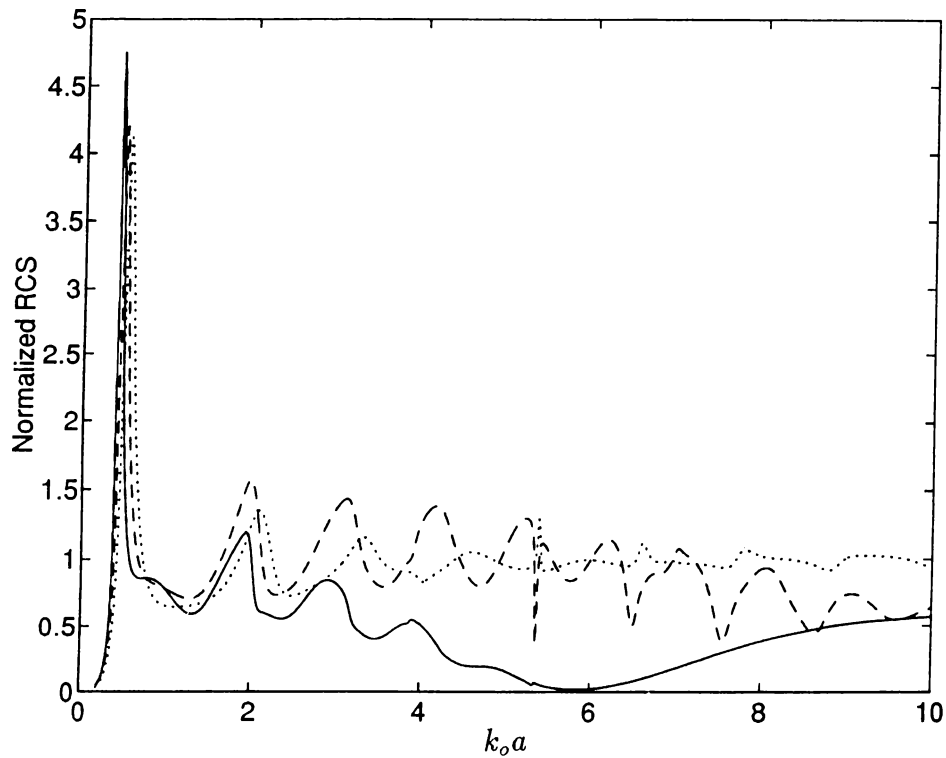
Figure 4.11: The normalized RCS of an uncoated and outer-coated CBA for H-pol incidence for two different absorbing materials with CBA having $60°$ aperture size, $\varphi_o = 0°$ and the coating radius b=1.1a; solid line: $\epsilon_r = 7.3$, $\mu_r = 0.91 + 0.32i$; dashed line: $\epsilon_r = 3.45 + 0.25i$, $\mu_r = 1$; dotted line: uncoated cylinder, i.e. $\epsilon_r = 1$, $\mu_r = 1$.
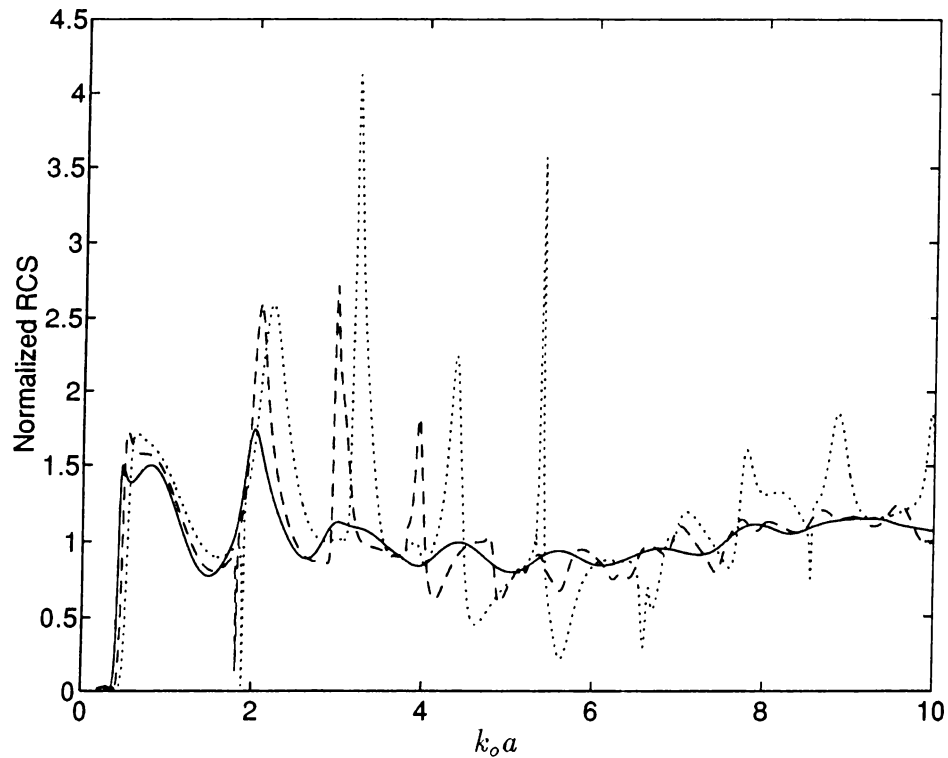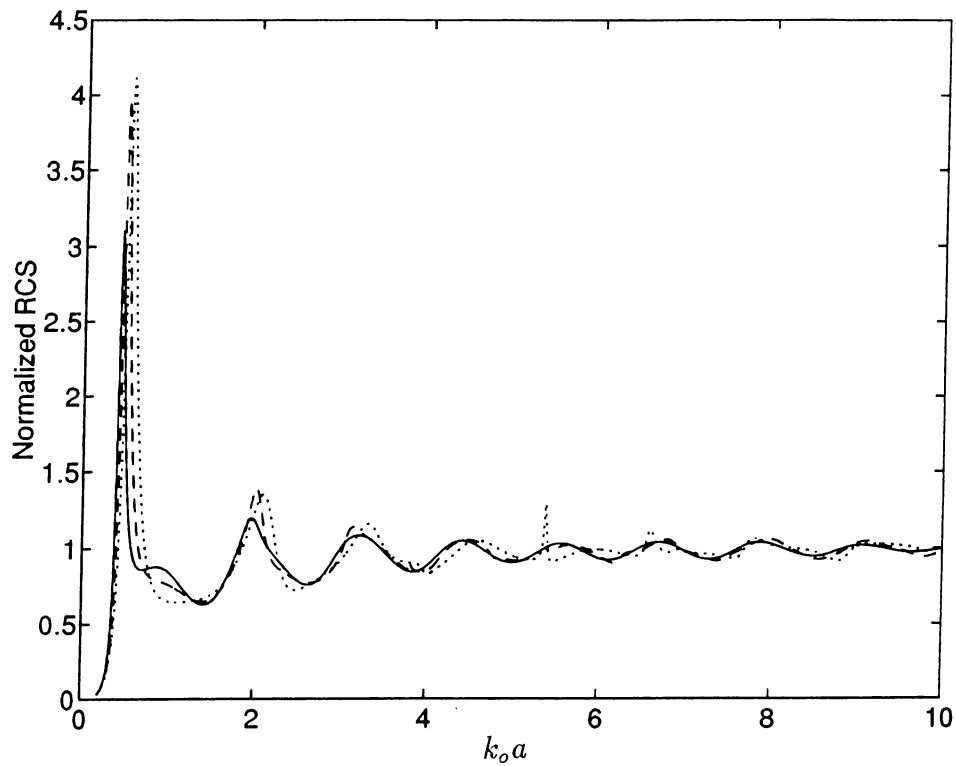
Figure 4.12: The normalized RCS of an uncoated and inner-coated CBA for H-pol incidence for two different absorbing materials with CBA having $60°$ aperture size, $\varphi_o = 0°$ and the coating radius b=0.9a; solid line: $\epsilon_r = 7.3$, $\mu_r = 0.91 + 0.32i$; dashed line: $\epsilon_r = 3.45 + 0.25i$, $\mu_r = 1$; dotted line: uncoated cylinder, i.e. $\epsilon_r = 1$, $\mu_r = 1$.

Figure 4.13: The normalized RCS versus aspect angle of the screen, i.e. $\varphi_o$, for E-pol. incidence for the magnetic absorbing material with $\epsilon_r = 7.3$, $\mu_r = 0.91 + 0.32i$ at $k_o a = 8$; solid line: Inner-coated CBA, dashed line: Outer-coated CBA, dotted line: uncoated cylinder, i.e. $\epsilon_r = 1$, $\mu_r = 1$.

## 4.2 RCS versus Aspect Angle of the Screen

### 4.2.1 E-polarized Case

The dependences of normalized RCS on the angle of aperture orientation $\varphi_o$ are presented in Figures 4.13 and 4.14 for two sample frequencies, namely $k_o a = 8.0$ (close to a local maximum RCS of uncoated CBA) and $k_o a = 8.5$ (close to a local minimum RCS of uncoated CBA). Only lossy magnetic coating results are given, for the same parameters of absorber as before. In spite of the fact that these two frequencies are close to each other, the RCS behaviors for uncoated CBA are quite different (dotted curves). This proves that numerical analysis of frequency scan is very important and must precede any study of RCS at fixed frequencies. One also notes that at on-aperture incidence, the

Figure 4.14: The normalized RCS versus aspect angle of the screen, i.e. $\varphi_o$, for E-pol. incidence for the magnetic absorbing material with $\epsilon_r = 7.3$, $\mu_r = 0.91 + 0.32i$ at $k_o a = 8.5$; solid line: Inner-coated CBA, dashed line: Outer-coated CBA, dotted line: uncoated cylinder, i.e. $\epsilon_r = 1$, $\mu_r = 1$.

inner coating (solid curves) serves much better for reducing the RCS, than outer one (dashed curves). As observed in Figures 4.1 and 4.2, when the wave hits the aperture directly, the effect of resonances makes the structure strongly frequency-dependent. Therefore, RCS dependence on the angle of orientation at two different frequencies, even they are close to each other, will be quite different. The same conclusion is also valid for off-resonance frequencies.

## 4.2.2 H-polarized Case

The dependences of normalized RCS on the angle of aperture orientation $\varphi_o$ are presented in Figures 4.15 and 4.16 for two sample frequencies, namely $k_o a = 6.94$ (close to a local minimum RCS for uncoated CBA) and $k_o a = 7.54$ (close to a local maximum RCS of uncoated CBA). One notes again that at
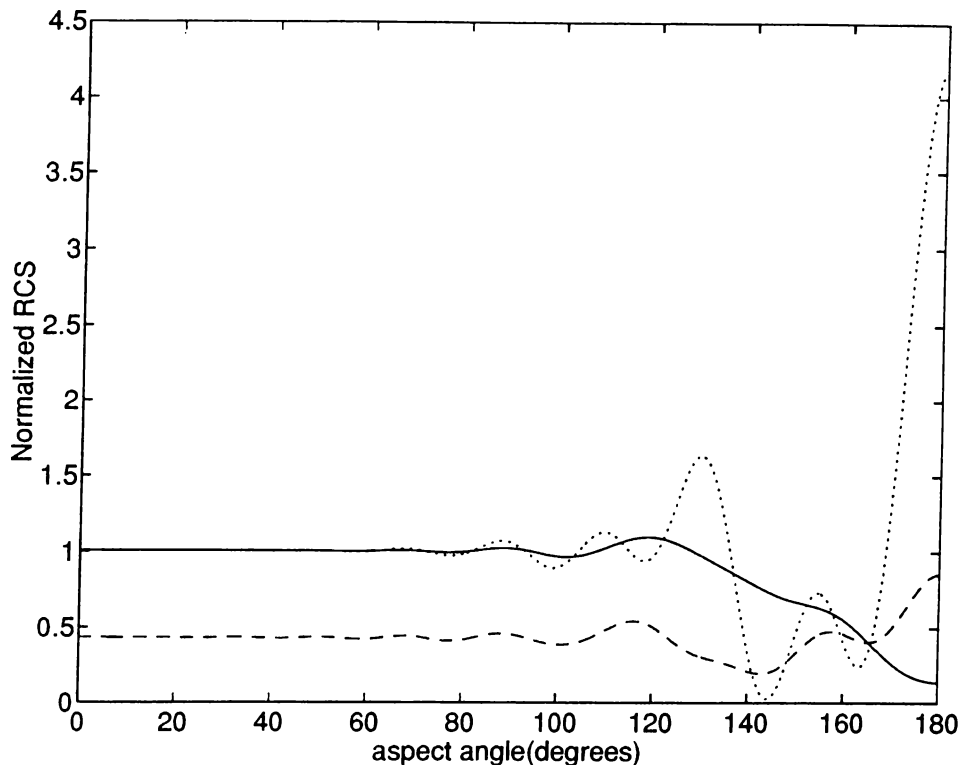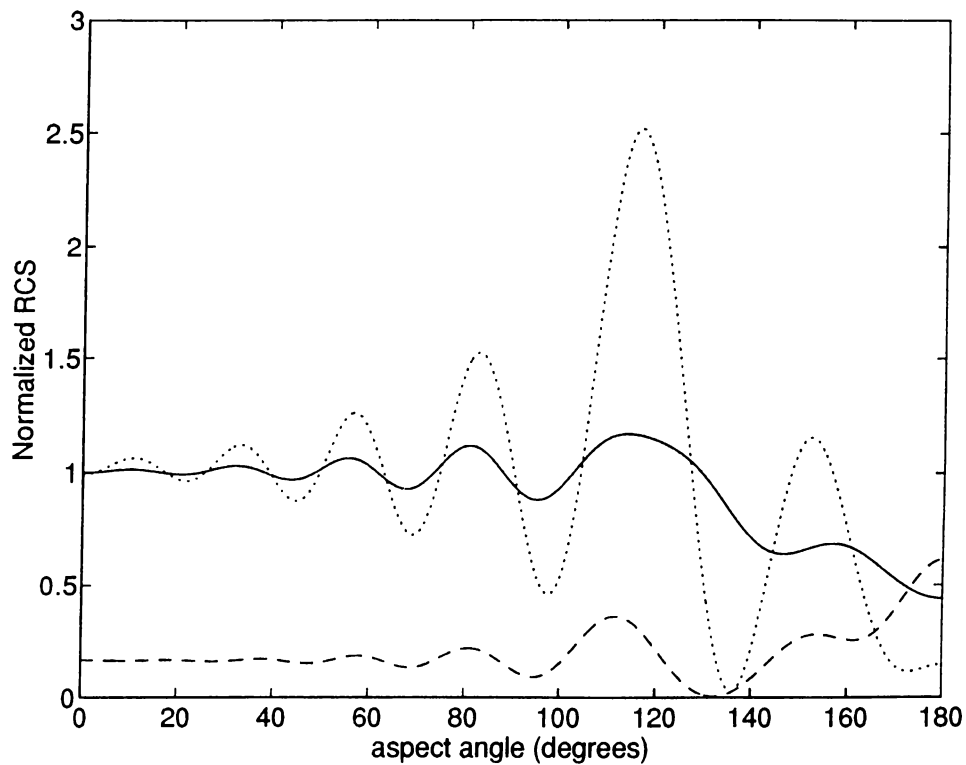
Figure 4.15: The normalized RCS versus aspect angle of the screen, i.e. $\varphi_o$, for H-pol. incidence for the magnetic absorbing material with $\epsilon_r = 7.3$, $\mu_r = 0.91 + 0.32i$ at $k_o a = 6.94$; solid line: Inner-coated CBA, dashed line: Outer-coated CBA, dotted line: uncoated cylinder, i.e. $\epsilon_r = 1$, $\mu_r = 1$.
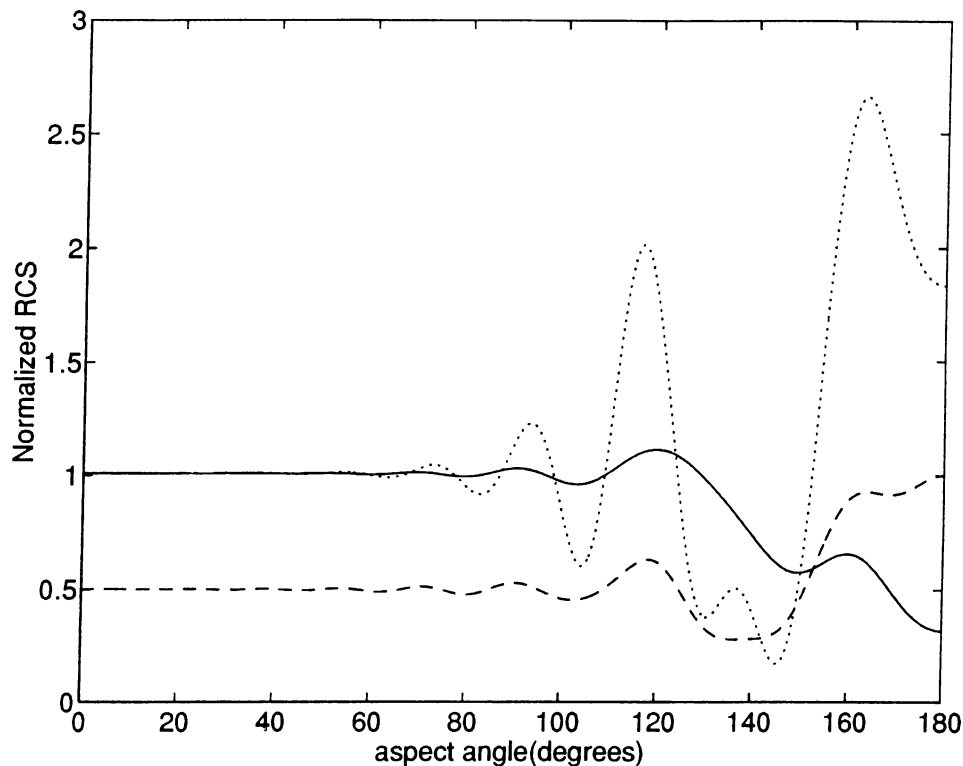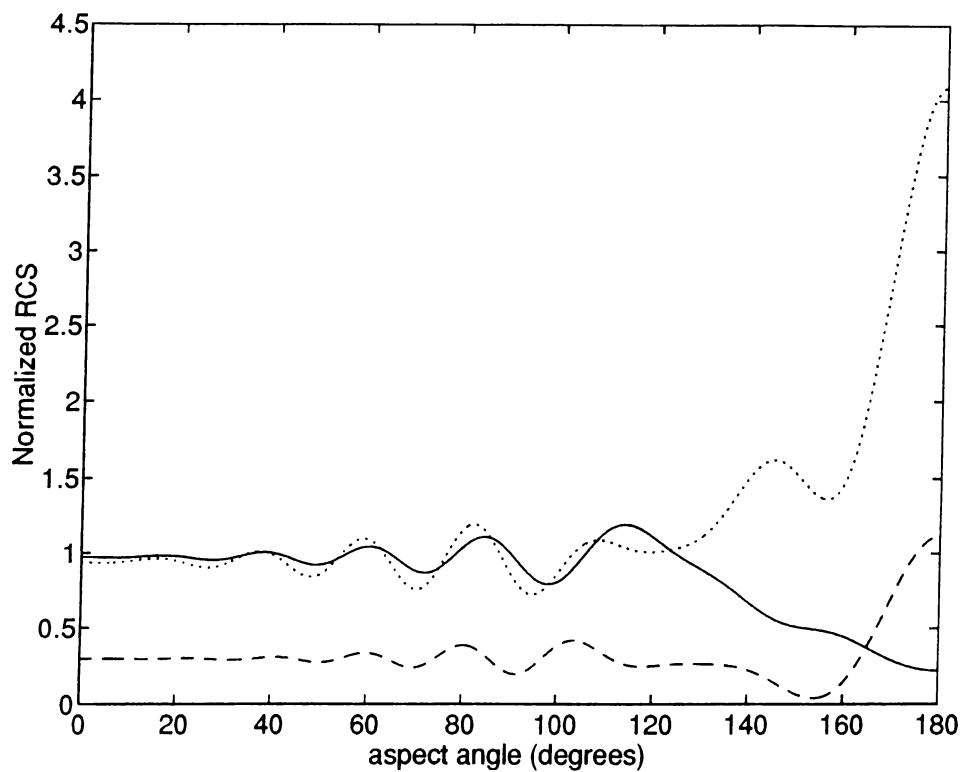
Figure 4.16: The normalized RCS versus aspect angle of the screen, i.e. $\varphi_o$, for H-pol. incidence for the magnetic absorbing material with $\epsilon_r = 7.3$, $\mu_r = 0.91 + 0.32i$ at $k_o a = 7.54$; solid line: Inner-coated CBA, dashed line: Outer-coated CBA, dotted line: uncoated cylinder, i.e. $\epsilon_r = 1$, $\mu_r = 1$.

Figure 4.17: The normalized RCS of an outer-coated CBA versus relative thickness of the layer, for E-pol incidence; CBA has $60°$ aperture size, $\varphi_o = 180°$ and $\epsilon_r = 7.3$, $\mu_r = 0.91 + 0.32i$; solid line: $k_o a = 9.39$; dashed line: $k_o a = 8.5$; dotted line: $k_o a = 1.71$.

on-aperture incidence, the inner coating (solid curves) serves much better for reducing the RCS, than outer one (dashed curves).

## 4.3 RCS versus Relative Thickness of the Absorbing Layer

### 4.3.1 E-polarized Case

The dependence of RCS on the thickness of the absorbing layer are presented in Figures 4.17 and 4.18, for outer and inner coating respectively. The results are obtained only for the lossy magnetic material for coating from inside

Figure 4.18: The normalized RCS of an inner-coated CBA versus relative thickness of the layer, for E-pol incidence; CBA has $60°$ aperture size, $\varphi_o = 180°$ and $\epsilon_r = 7.3$, $\mu_r = 0.91 + 0.32i$; solid line: $k_o a = 9.39$; dashed line: $k_o a = 8.5$; dotted line: $k_o a = 1.71$.

and from outside at some specific frequencies, namely for $k_o a = 1.71$ (dotted curves), $k_o a = 8.5$, (dashed curves) and $k_o a = 9.39$ (solid curves). As "$b$" approaches to "$a$", RCS approaches to the value for the uncoated CBA response at those frequencies (see Figures 4.17 and 4.18). As seen from the figures, the curves have an oscillation at first, and then stabilize as the thickness is increased. Mainly, there are two mechanisms involved. The first one is the interference of the waves reflected from both surfaces of the material coating at the aperture, and the second one is the absorption inside the coating. The former prevails when the thickness is small and the latter when it is larger. The location of the minima in Figure 4.17 and 4.18 are in good agreement with the calculated ones for a lossy material slab of parameters $t$, $\epsilon_r$, and $\mu_r$, especially for higher frequencies. This validates the above explanation, since our circularly curved material coating is closer to a planar slab for higher frequencies. Hence, for the practical purposes, the thickness of the dielectric slab
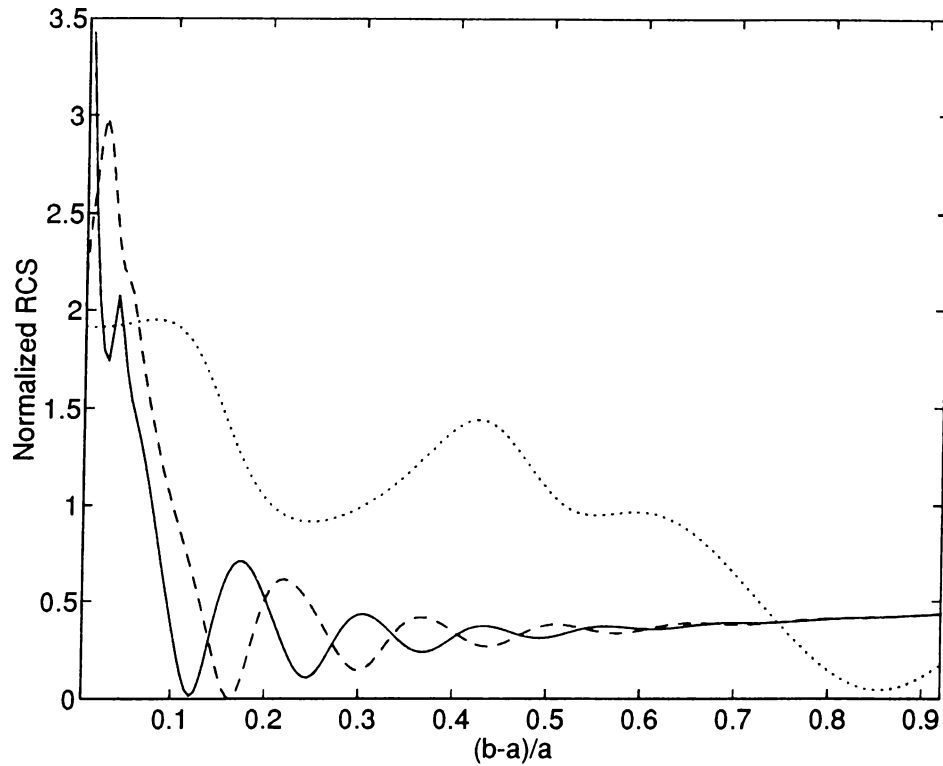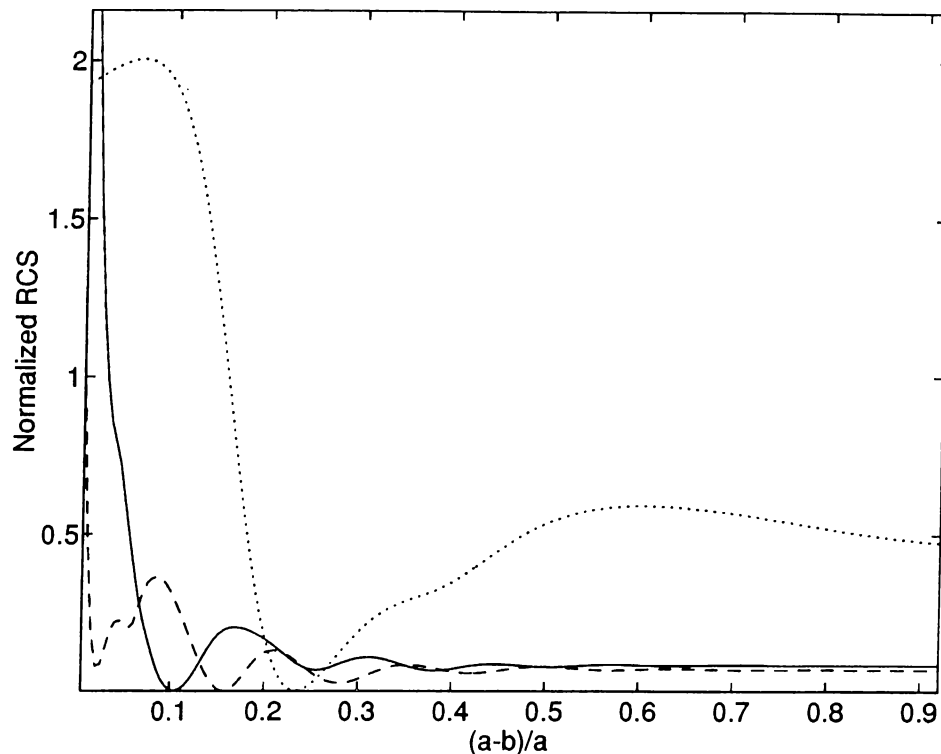
Figure 4.19: The normalized RCS of an outer-coated CBA versus relative thickness of the layer, for H-pol incidence; CBA has $60°$ aperture size, $\varphi_o = 180°$ and $\epsilon_r = 7.3$, $\mu_r = 0.91 + 0.32i$; solid line: $k_o a = 9.39$; dashed line: $k_o a = 8.5$; dotted line: $k_o a = 1.71$.

can be chosen so that RCS has a minimum value at a specified frequency. On the other hand, if the absorbing layer were covering only the walls of CBA, but not the aperture itself, one could expect the absence of interference minima in Figures 4.17 and 4.18.

## 4.3.2   H-polarized Case

The dependence of RCS on the thickness of the absorbing layer is presented in Figures 4.19 and 4.20 for coating from outside and from inside, respectively, with lossy magnetic material, and for the case of aperture in the illuminated region. There are again oscillations in the RCS for lower thickness values and then stabilizes as the thickness is increased. This can be explained in the same way that is proposed in E-pol. case.
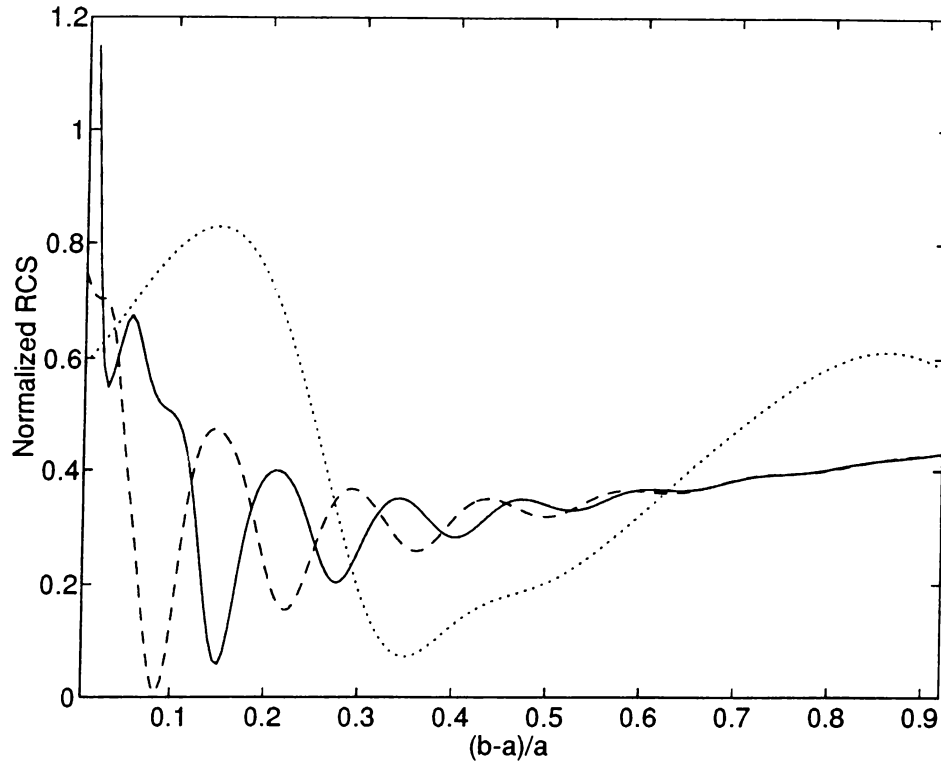
48
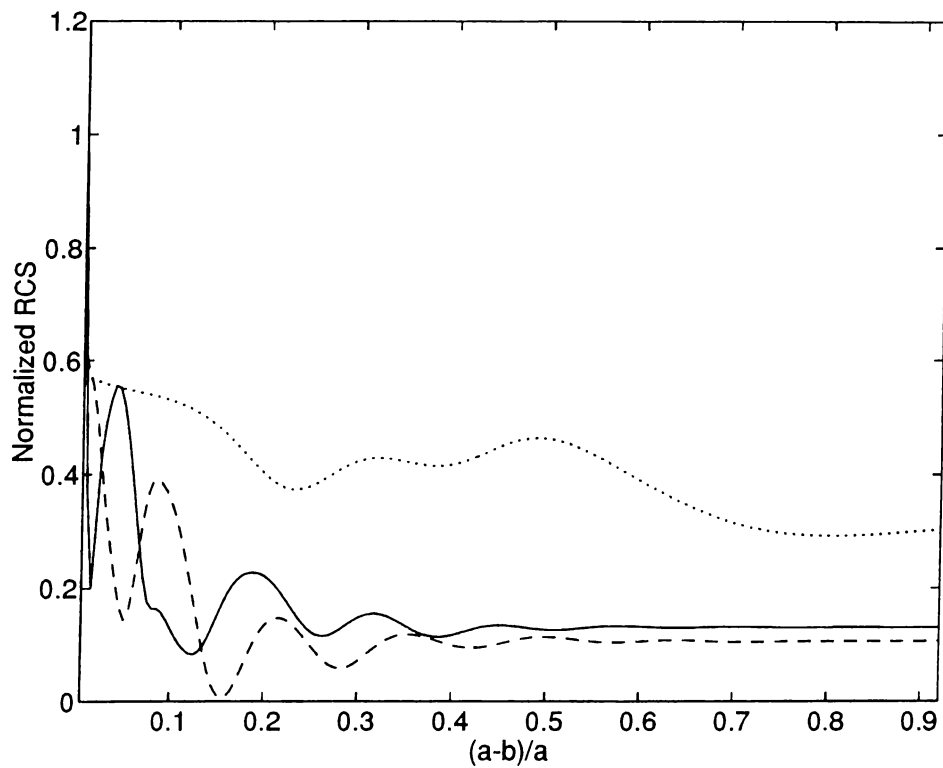
Figure 4.20: The normalized RCS of an inner-coated CBA versus relative thickness of the layer, for H-pol incidence; CBA has $60°$ aperture size, $\varphi_o = 180°$ and $\epsilon_r = 7.3$, $\mu_r = 0.91 + 0.32i$; solid line: $k_o a = 9.39$; dashed line: $k_o a = 8.5$; dotted line: $k_o a = 1.71$.

49
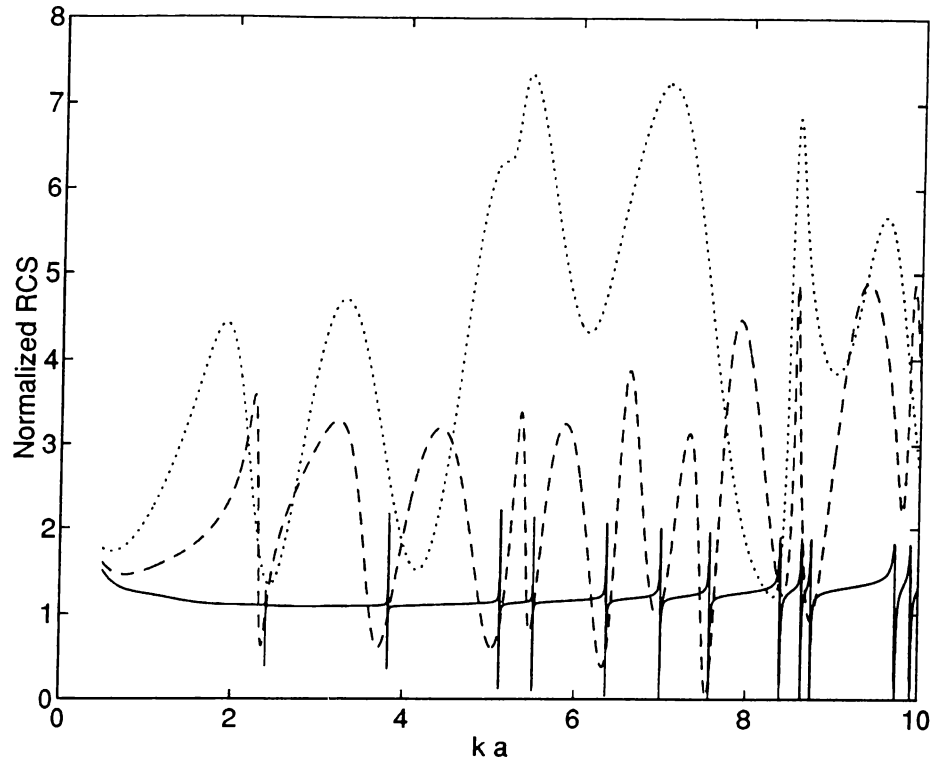
Figure 4.21: The normalized RCS of an uncoated CBA having three different aperture sizes, $\varphi_o = 180°$, for E-pol incidence; solid line: $\theta = 5°$; dashed line: $\theta = 30°$; dotted line: $\theta = 60°$.

## 4.4 RCS for Various Aperture Sizes

### 4.4.1 E-Polarized Case

The dependence of RCS on the aperture size is presented in Figure 4.21 for uncoated CBA. It is observed that, as the size of the aperture increases, the resonant frequencies decrease and the bandwidth increases. The physical interpretation is as follows. The field inside the cavity extends to the outside through the aperture opening. It can also be interpreted as the loss of energy. Therefore, as the aperture opening size increases, the energy loss also increases which leads to broadening of the resonance spikes, i.e. quality factor of the resonant spike decreases. The decrease in resonance frequency is also consistent with equations (4.1) and (4.2).

The effect of coating on the outer and inner walls of the screen for $\theta = 5°$

Figure 4.22: The normalized RCS of an uncoated and outer-coated CBA for E-pol. incidence for two different absorbing materials with CBA having $10°$ aperture size, $\varphi_o = 180°$ and the coating radius b=1.1a; solid line: $\epsilon_r = 7.3$, $\mu_r = 0.91 + 0.32i$; dashed line: $\epsilon_r = 3.45 + 0.25i$, $\mu_r = 1$; dotted line: uncoated cylinder, i.e. $\epsilon_r = 1$, $\mu_r = 1$.

(aperture size of $10°$) and $\theta = 60°$ (aperture size of $120°$) is demonstrated in Figures 4.22 through 4.25 for the case of on-aperture incidence. Similar results are obtained as in the case of $\theta = 30°$ in Figures 4.1 and 4.2.

51

Figure 4.23: The normalized RCS of an uncoated and inner-coated CBA for E-pol. incidence for two different absorbing materials with CBA having $10°$ aperture size, $\varphi_o = 180°$ and the coating radius b=0.9a; solid line: $\epsilon_r = 7.3$, $\mu_r = 0.91 + 0.32i$; dashed line: $\epsilon_r = 3.45 + 0.25i$, $\mu_r = 1$; dotted line: uncoated cylinder, i.e. $\epsilon_r = 1$, $\mu_r = 1$.

Figure 4.24: The normalized RCS of an uncoated and outer-coated CBA for E-pol. incidence for two different absorbing materials with CBA having $120°$ aperture size, $\varphi_o = 180°$ and the coating radius b=1.1a; solid line: $\epsilon_r = 7.3$, $\mu_r = 0.91 + 0.32i$; dashed line: $\epsilon_r = 3.45 + 0.25i$, $\mu_r = 1$; dotted line: uncoated cylinder, i.e. $\epsilon_r = 1$, $\mu_r = 1$.
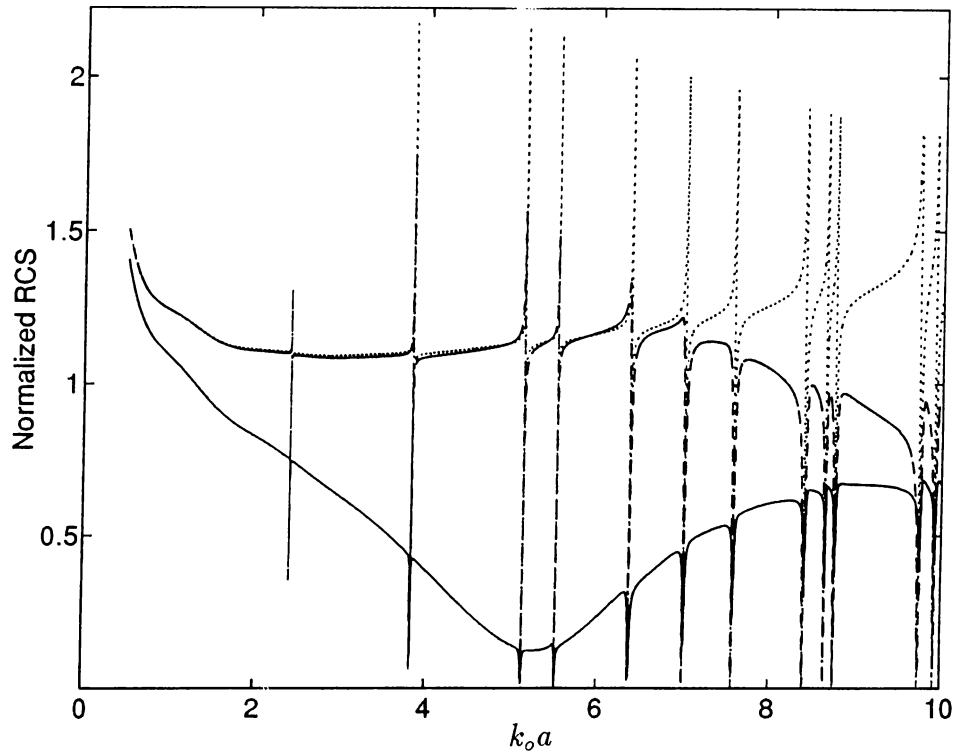
Figure 4.25: The normalized RCS of an uncoated and inner-coated CBA for E-pol. incidence for two different absorbing materials with CBA having $120°$ aperture size, $\varphi_o = 180°$ and the coating radius b=0.9a; solid line: $\epsilon_r = 7.3$, $\mu_r = 0.91 + 0.32i$; dashed line: $\epsilon_r = 3.45 + 0.25i$, $\mu_r = 1$; dotted line: uncoated cylinder, i.e. $\epsilon_r = 1$, $\mu_r = 1$.

Figure 4.26: The normalized RCS of an uncoated CBA having three different aperture sizes, $\varphi_o = 180°$, for H-pol incidence; solid line: $\theta = 5°$; dashed line: $\theta = 30°$; dotted line: $\theta = 60°$.

## 4.4.2 H-Polarized Case

The dependence of RCS on the aperture size is presented in Figure 4.26 for uncoated CBA. Contrary to E-pol. case, as the opening increases, the resonant frequencies also increase as seen in Figure 4.26. This is consistent with the formulas (4.6) and (4.7). One also notes that, as the size of the opening increases, the bandwidth also increases which is the same observation in the E-pol. case.

The effect of coating on the outer and inner walls of the screen for $\theta = 5°$ and $\theta = 60°$ is demonstrated in Figures 4.27 through 4.30 for the case of on-aperture incidence. Similar results are obtained as in the case of $\theta = 30°$ in Figures 4.7 and 4.8.
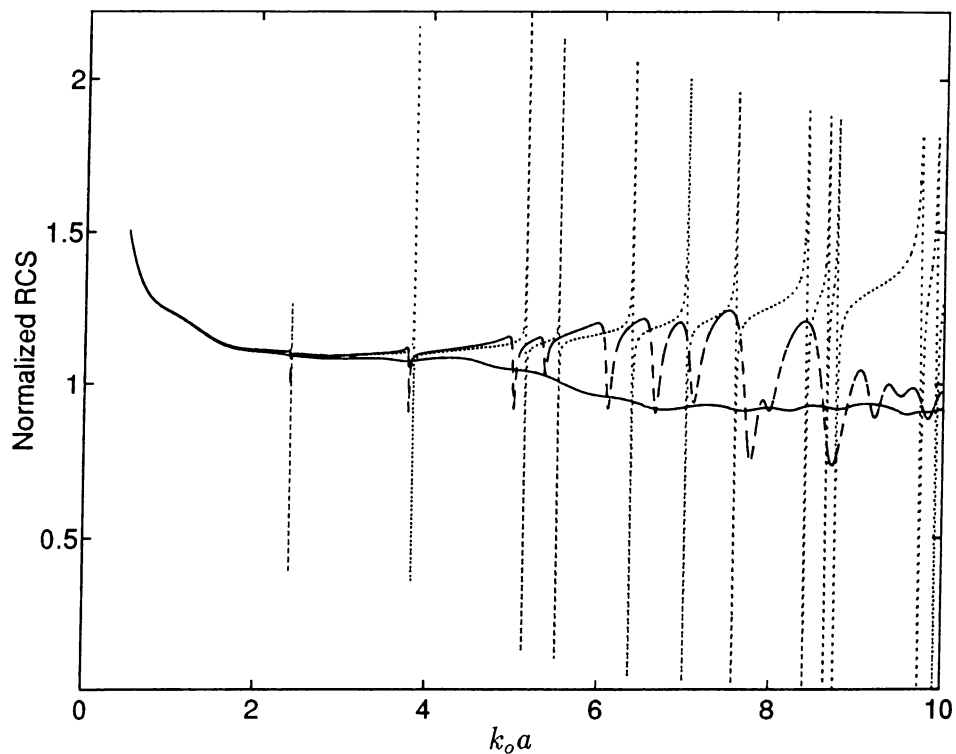
Figure 4.27: The normalized RCS of an uncoated and outer-coated CBA for H-pol. incidence for two different absorbing materials with CBA having $10°$ aperture size, $\varphi_o = 180°$ and the coating radius b=1.1a; solid line: $\epsilon_r = 7.3$, $\mu_r = 0.91 + 0.32i$; dashed line: $\epsilon_r = 3.45 + 0.25i$, $\mu_r = 1$; dotted line: uncoated cylinder, i.e. $\epsilon_r = 1$, $\mu_r = 1$.
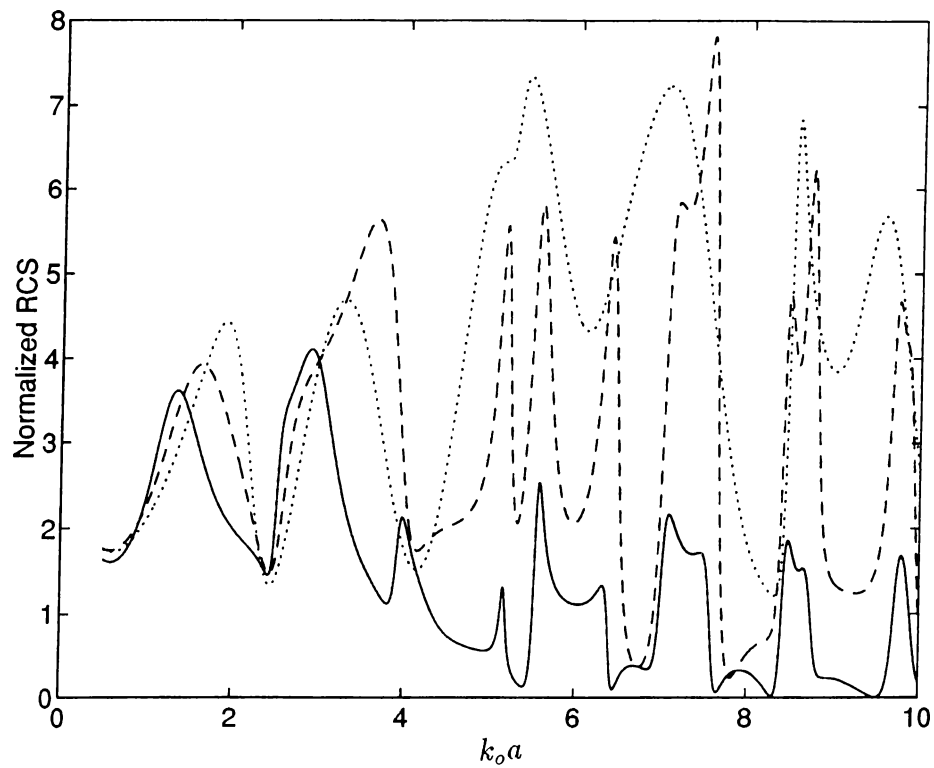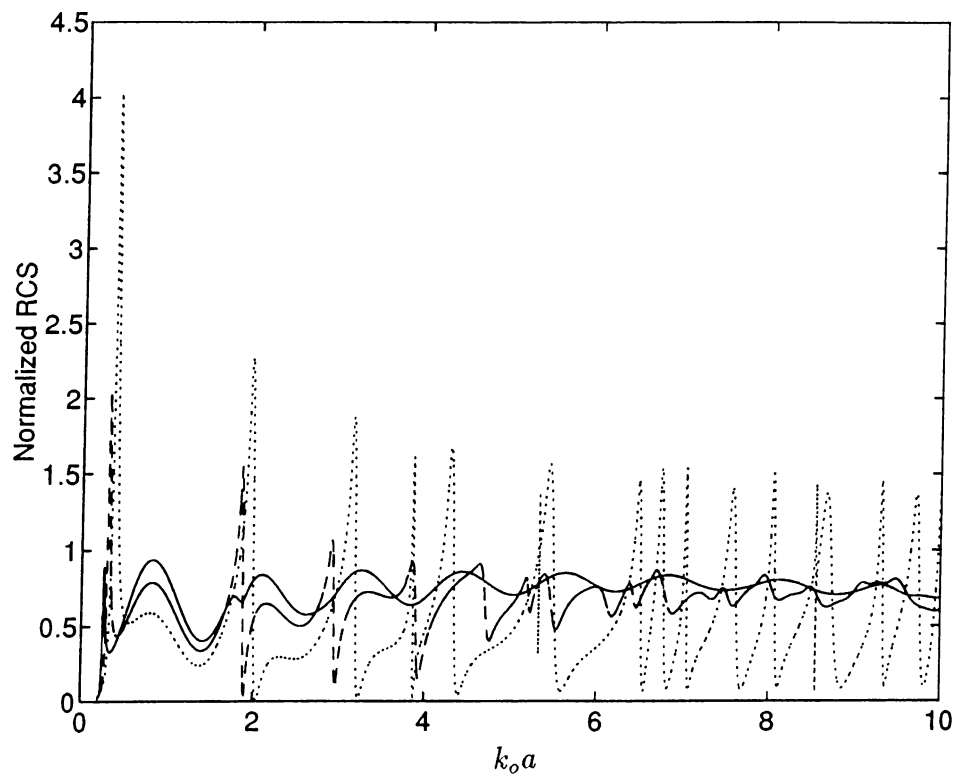
Figure 4.28: The normalized RCS of an uncoated and inner-coated CBA for H-pol. incidence for two different absorbing materials with CBA having $10°$ aperture size, $\varphi_o = 180°$ and the coating radius b=0.9a; solid line: $\epsilon_r = 7.3$, $\mu_r = 0.91 + 0.32i$; dashed line: $\epsilon_r = 3.45 + 0.25i$, $\mu_r = 1$; dotted line: uncoated cylinder, i.e. $\epsilon_r = 1$, $\mu_r = 1$.
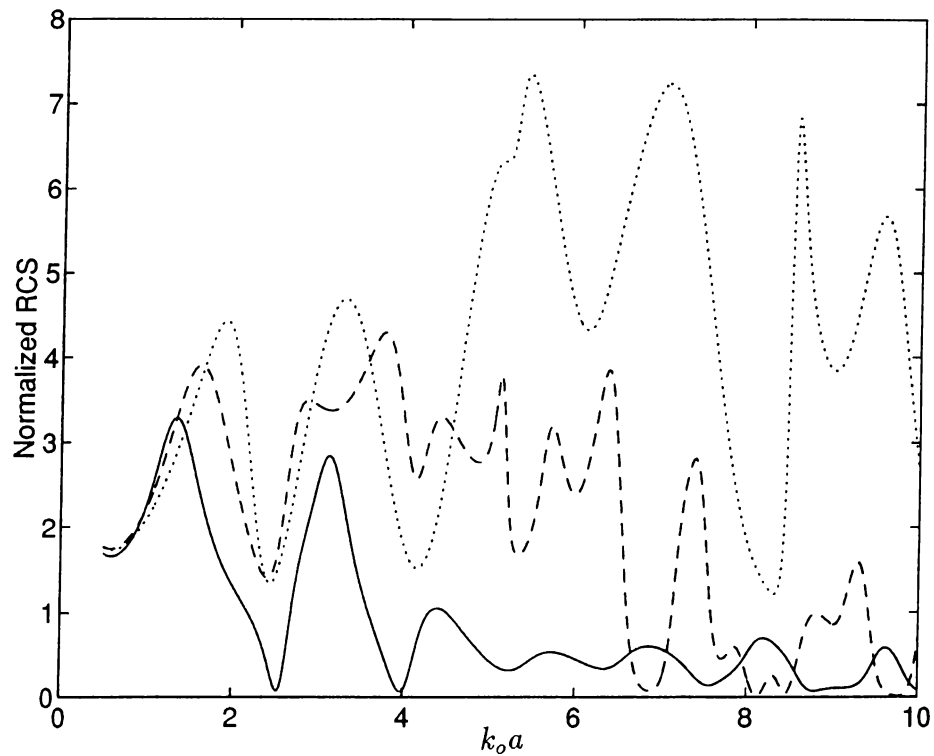
57
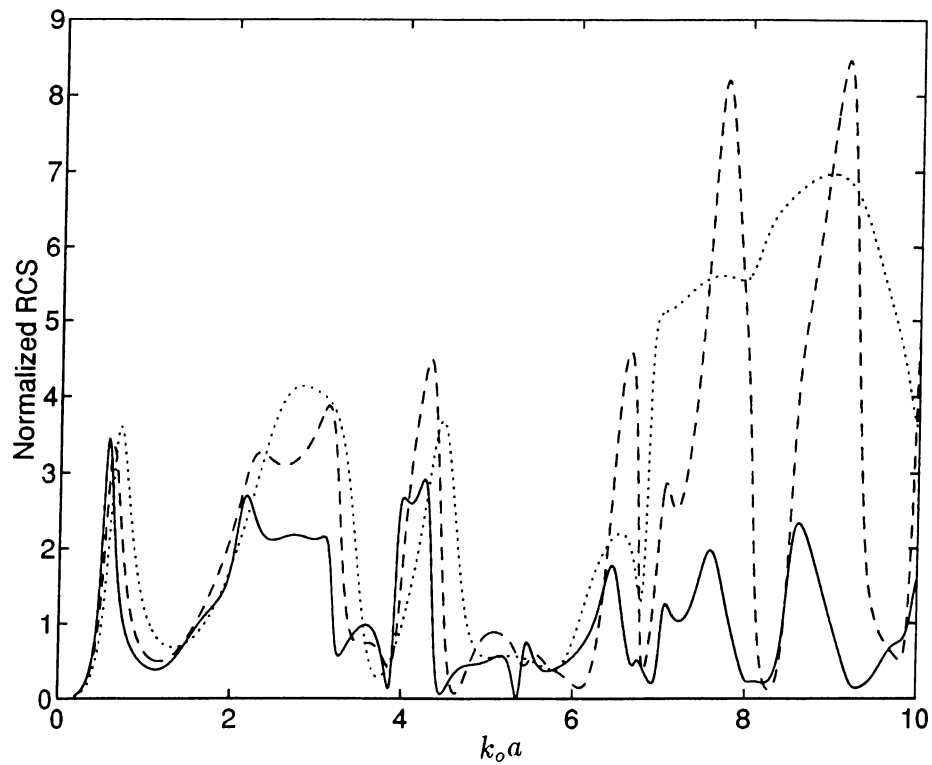
Figure 4.29: The normalized RCS of an uncoated and outer-coated CBA for H-pol. incidence for two different absorbing materials with CBA having $120°$ aperture size, $\varphi_o = 180°$ and the coating radius b=1.1a; solid line: $\epsilon_r = 7.3$, $\mu_r = 0.91 + 0.32i$; dashed line: $\epsilon_r = 3.45 + 0.25i$, $\mu_r = 1$; dotted line: uncoated cylinder, i.e. $\epsilon_r = 1$, $\mu_r = 1$.
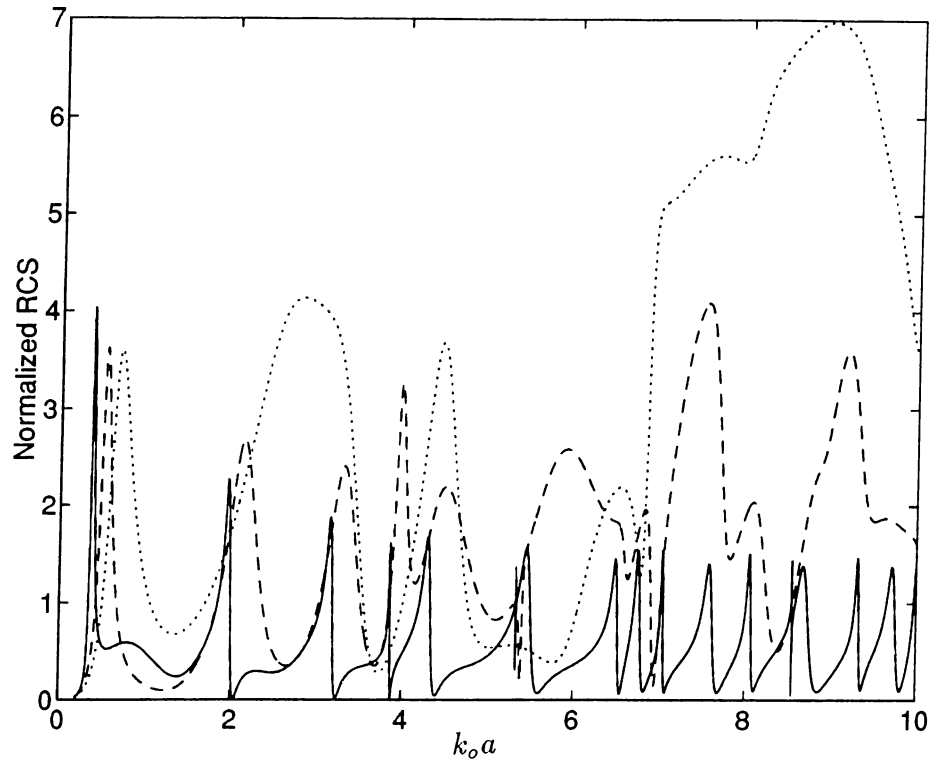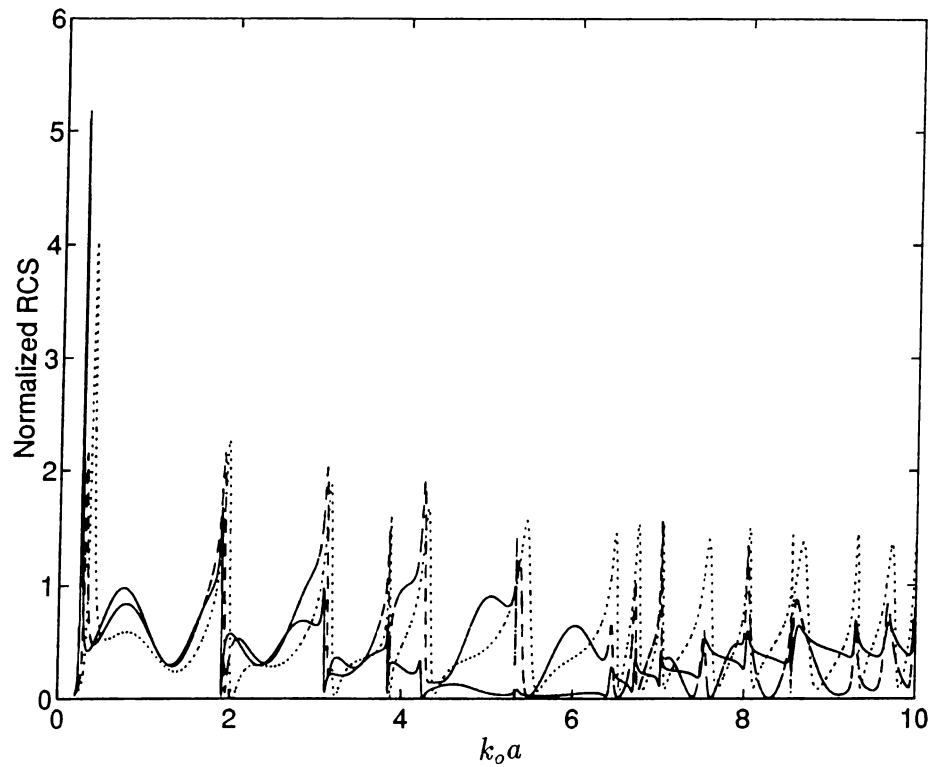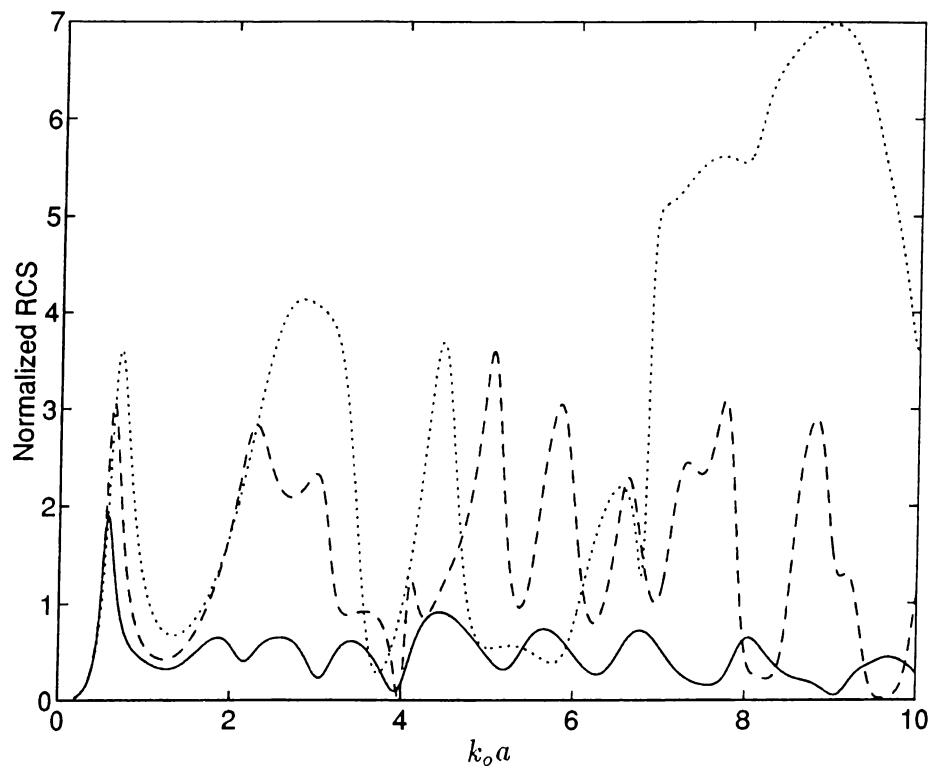
Figure 4.30: The normalized RCS of an uncoated and inner-coated CBA for H-pol. incidence for two different absorbing materials with CBA having 120° aperture size, $\varphi_o = 180°$ and the coating radius b=0.9a; solid line: $\epsilon_r = 7.3$, $\mu_r = 0.91 + 0.32i$; dashed line: $\epsilon_r = 3.45 + 0.25i$, $\mu_r = 1$; dotted line: uncoated cylinder, i.e. $\epsilon_r = 1$, $\mu_r = 1$.

# Chapter 5

# CONCLUSION

In this thesis, we considered the problem of electromagnetic wave scattering from a thin, perfectly conducting, slitted infinite cylinder which is coated with absorbing material either from inside or from outside. To the best of our knowledge, this is the first study made so far to solve the problems of CBAs with non-homogeneous space inside or outside with this approach.

The problem is first reduced into dual series equations and then solved by using RHP technique of complex variable theory. Since the final matrix equations are proven to be of Fredholm second kind, one can be sure about the existence and uniqueness of the solution and the solution can be obtained with any desired accuracy. Therefore, the numerical results obtained can serve a reference data for more complicated scatterers.

Numerical results are obtained for radar cross section (RCS) as a function of frequency for different coating materials and different orientation of the aperture. Also, presented are dependence of RCS on the relative thickness of the absorbing layer and on the aspect angle of the screen. Finally, dependence on the aperture size of the screen is presented numerically. The results generated for E-pol incidence are compared with those generated for H-pol. incidence.

According to our numerical results, the lossy magnetic material results in a better reduction of resonances in RCS behavior of the CBA. Further, it is much better to make coating from inside to suppress the resonances when the interior resonance is the dominant feature in the back scattering characteristics. In the case of direct on aperture incidence, the inner coating is better at any

frequency. On the other hand, coating from outside can be preferred to reduce the average level of the RCS, but it has no effect on the internal resonances. The dependence of RCS on the aperture size is examined numerically and comparison is made for both polarizations. Finally, it is possible to adjust the thickness of the absorbing layer at a specific frequency so that RCS has a minimum value.

For future research, we can study on non-perfect conductors by RHP technique by making impedance surface modeling. Also, impedance-surface CBA on a periodic material interface can also be solved with this approach.

# Appendix A

## COEFFICIENT DEFINITION

In this appendix, the coefficient $T_{mn}$ is defined. $T_{mn}(u)$ is related to the Legendre polynomials, $P_n(u)$ through the following expressions

$$T_{mn}(u) = \begin{cases} Q_{mn}(u), & m \neq 0 \\ Q_{n0}(u), & m = 0, n \neq 0 \\ -\ln[(1+u)/2], & m = n = 0 \end{cases} \qquad (A.1)$$

where

$$Q_{mn}(u) = \frac{1}{2(m-n)}[P_{m-1}(u)P_n(u) - P_m(u)P_{n-1}(u)], \quad m \neq n$$

$$Q_{mm}(u) = \frac{sign(m)}{2m} \sum_{s=0}^{|m|} q_{|m|-s}(u)P_{|m|-s-1}(u),$$

$$q_o(u) = 1, q_1(u) = -u, \dots \quad q_s(u) = P_s(u) - 2uP_{s-1}(u) + P_{s-2}(u)$$

and we make use of the relation $P_{-s-1}(u) = P_s(u)$.

# Appendix B

## NATURAL MODES OF OSCILLATIONS OF UNCLOSED CIRCULAR CYLINDRICAL SHELL

Natural modes of oscillations are obtained by assuming $E^{in} = H^{in} = 0$ for the incident field.

Consider free oscillations of H-type. As in the diffraction, $H_z^{sc}$ can be represented by a double layer potential as

$$H_z^{sc}(\vec{r}) = \int_M \mu(\vec{r}\prime) \frac{\partial G_o(\vec{r}, \vec{r}\prime)}{\partial n\prime}\, d\vec{r}\prime$$

where $\mu(\vec{r})$ is the unknown current density and $n$ is the outward unit normal vector. The current density is discretized in terms of angular exponents $e^{in\varphi}, n = 0, \pm 1, \cdots$ as

$$\mu(\vec{r}) = \frac{2}{i\pi k_o a} \sum_{(n)} \mu_n e^{in\varphi} \ .$$

Besides, by employing addition theorem of the cylindrical functions, we have

$$G_o(\vec{r}, \vec{r}\prime) = \frac{i}{4} \sum_{(n)} \left\{ \begin{array}{ll} J_n(kr\prime)H_n^{(1)}(kr) & r > r\prime \\ J_n(kr)H_n^{(1)}(kr\prime) & r < r\prime \end{array} \right\} e^{in(\varphi - \varphi\prime)}$$

After imposing the boundary conditions, one can obtain a homogeneous system of functional dual series equations for the coefficients $\mu_n$ . The RHP technique as described in the second chapter yields homogeneous matrix equations for even and odd electromagnetic fields,

$$\mu_m = \frac{1}{2} \sum_{n=0}^{\infty} \tau_n (A_{mn} + A_{-mn}) \mu_n$$

$$\mu_{-m} = \sum_{n=1}^{\infty} (A_{mn} - A_{-mn}) \mu_{-n}$$

respectively, where $\tau_n = 1$ for $n = 0$ and $\tau = 2$ for $n > 0$.

Equating the determinants of these matrices to zero yields the characteristic equation for determining the resonance frequencies of even

$$\mid \delta_m^n - \frac{1}{2} \tau_n (A_{mn} + A_{-mn}) \mid_{m,n=0}^{\infty} \tag{B.1}$$

and of odd type of oscillations

$$\mid \delta_m^n - \frac{1}{2} \tau_n (A_{mn} - A_{-mn}) \mid_{m,n=1}^{\infty} \tag{B.2}$$

where $\delta_m^n$ is the Kronecker delta.

Since it is proved in [14] that

$$\sum_{m,n} \mid A_{mn} \pm A_{-mn} \mid < \infty \ ,$$

the characteristic equation can be solved through truncation with any desired accuracy.

In case the slot is narrow ($\theta \to 0$), the matrices are close to diagonal one. Therefore the complex roots of the characteristic equation can be obtained analytically as an asymptotic power series which is dependent on the opening width, $2\theta$.

The asymptotic behavior of $A_{mn}$ and $A_{-mn}$ for small $\theta$ is examined and it is found that the matrix in (B.1) has nonzero elements at the main diagonal, at zeroth row and column, and remaining cells have values proportional to $\theta^2$. Similarly, the matrix in (B.2) has nonzero elements only at the main diagonal. Therefore the iterative-perturbation analysis is applicable (see [14]). Hence, the roots of the characteristic equation are approximately found as,

$$k_{mn}^+ a \approx \nu_{mn} + \nu_{mn} \left[ \delta_m (\nu_{mn}^2 - m^2) ln\tau \right]^{-1} (1 + i\zeta_{mn} ln^{-1}\tau), \tag{B.3}$$

for the even modes ($m = 1, 2, ...$), and

$$k_{mn}^- a \approx \nu_{mn} + \nu_{mn} m^2 (\nu_{mn}^2 - m^2)^{-1} \tau^2 (1 - 2i\Upsilon_{mn}\tau^2) \tag{B.4}$$

64

for the odd modes ($m = 1, 2, ...$) of the empty circular slitted cavity. In (B.3) and (B.4),

$$\zeta_{mn} = \pi^{-1}\nu_{mn}^{-2} \sum_{s=\neq 0,m}^{\infty} |H_s'(\nu_{mn})|^{-2}, \quad \Upsilon_{mn} = \pi^{-1}\nu_{mn}^{-2} \sum_{s=1,\neq m}^{\infty} s^2|H_s'(\nu_{mn})|^{-2}$$

(B.5)

and $\delta_o = 1, \delta_s = 2$ for $s \neq 0$, and $\nu_{mn}$ is the n-th zero of $J_m'(x)$.

The details of this analysis are given in [14].

# REFERENCES

[1] A. Altıntaş, P. H. Pathak, and M. C. Liang, "A Selective Modal Scheme for the Analysis of EM Coupling Into or from Large Open-Ended Waveguides," *IEEE Trans. Antennas Propagat.,*vol. AP-36, No. 1, pp. 84-96, Jan. 1988.

[2] A. Altıntaş, "Electromagnetic Scattering from a Class of Open-Ended Waveguide Discontinuities," Ph.D. dissertation, Dept. Elect. Eng., Ohio State Univ., Columbus, Mar. 1986.

[3] C. S. Lee and S. W. Lee, "RCS of a Coated Circular Waveguide Terminated by a Perfect Conductor," *IEEE Trans. Antennas Propagat.,* vol. AP-35,No. 4, pp. 391-398, Apr. 1987.

[4] N. H. Myung, " A High Frequency Analysis of Electromagnetic Plane Wave Scattering by Perfectly-Conducting Semi-Infinite Parallel-Plate and Rectangular Waveguides with Absorber Coated Inner Walls," Ph.D. dissertation, Dept. Elect. Eng., Ohio State Univ., Columbus, 1986.

[5] H. Ling, R. C. Chou, and S. W. Lee, " Shooting and Bouncing Rays: Calculating the RCS of an Arbitrarily Shaped Cavity," *IEEE Trans. Antennas Propagat.,* vol. AP-37, No2, pp. 194-205, Feb. 1989.

[6] H. Shirai and L. B. Felsen, " Rays, Modes and Beams for Plane Wave Coupling into a Wide Open-ended Parallel-plane Waveguide," *Wave Motion,* vol. 9, pp. 301-317, 1987.

[7] K. Kobayashi, and A.Sawai, "Plane Wave Diffraction by an Open-Ended Parallel-Plate Waveguide Cavity", *J. Electromag. Waves Appl.,* vol. 6, pp. 475-512, 1992.

[8] L. B. Felsen and G. Vecchi, "Wave Scattering from Slit Coupled Cylindrical Cavities with Interior Loading: Part II-Resonant Mode Expansion,"

*IEEE Trans.Antennas Propagat.,*vol AP-39, No. 8, pp. 1085-1097, August 1991

[9] R. F. Harrington, and J. R. Mautz, "A Generalized Network Formulation for Aperture Problems," *IEEE Trans. Antennas Propagat.,* vol AP-24, pp.870-873, Nov. 1976.

[10] J. R. Mautz, and R. F. Harrington, "Electromagnetic Penetration into a Conducting Circular Cylinder Through a Narrow Slot, TE Case", *J. Electromagn. Waves Appl.,* vol. 3, No.4, pp. 307–336, 1989.

[11] A. El-Hajj, K. Y. Kabalan, and R. F. Harrington, " Characteristic Modes of a Slot in a Conducting Cylinder and Their Use for Penetration and Scattering, TE Case," *IEEE Trans.Antennas Propagat.,* vol AP-40, No. 2, pp. 156-161, Feb. 1992.

[12] Z. S. Agranovich, V. A. Marchenko and V. P. Shestopalov, " Diffraction of a Plane Electromagnetic Wave from Plane Metallic Lattices," *Soviet Physics-Tech. Physics.,* vol. 7, pp. 277-286, 1962.

[13] A. I. Nosich, " Green's Function-Dual Series Approach in Wave Scattering by Combined Resonant Scatterers", in M. Hashimoto, M. Idemen and O.A. Tretyakov (eds.), *Analytical and Numerical Methods in EM Wave Theory,* Tokyo, Science House, 1992

[14] A. I. Nosich, "Electromagnetic Characterization of Unclosed Circular Cylindrical Screens," Ph.D. Dissertation, Kharkov University,1979 (in Russian)

[15] W. A. Johnson and R. W. Ziolkowski, "The Scattering of an H-Polarized Plane Wave from an Axially Slotted Infinite Cylinder: A Dual Series Approach," *Radio Science,* vol. 19, No.1, pp. 275–291, Jan. 1984.

[16] R. W. Ziolkowski, "N-series Problems and the Coupling of Electromagnetic Waves to Apertures: A Riemann-Hilbert Approach, "*Soc. Industrial Appl. Math.,* vol. 16,no. 2, 1985

[17] R. W. Ziolkowski and J. B. Grant, " Scattering from Cavity-Backed Apertures: The Generalized Dual Series Solution of the Concentrically Loaded E-Pol Slit Cylinder Problem," *IEEE Trans.Antennas Propagat.,,* vol. AP-35, No.5, pp. 504-528, May 1987.

[18] R. W. Ziolkowski, W. A. Johnson, and K. F. Casey, "Applications of Riemann-Hilbert Problem Techniques to Electromagnetic Coupling Through Apertures," *Radio Science,* vol. 19, No. 6, pp. 1425–1431, Nov. 1984.

[19] A. I. Nosich and V. P. Shestopalov, " An electromagnetic analog of a Helmholtz Resonator,"*Sov. Phys. Dokl.* , pp. 251-253, May 1977.

[20] J. R. Mautz, and R. F. Harrington, "EM Penetration into a Conducting Circular Cylinder Through a Narrow Slot, TM Case", *J. Electromagn. Waves Appl.,* vol. 2, No.3/4, pp. 269–293, 1988.

[21] O. G. Gamulya, and A. I. Nosich, "Scattering Cross Sections and Ponderomotive Forces at the Diffraction of E-polarized Plane Wave from an Open Circular Screen", *Preprint No 326,* IRE-Kharkov Press, 1986 (in Russian).

[22] D. Çolak, A. I. Nosich and A. Altıntaş, "Radar Cross Section Study of Cylindrical Cavity-Backed Apertures with Outer or Inner Material Coating: The Case of E-Polarization," *IEEE Trans. Antennas Propagat.,* to be published.

[23] T. M. Wang and H. Ling, "Resonant Behavior of Conducting Slotted Rectangular Shell," *Microwave Opt. Tech. Lett.,* vol. 1, pp. 320-323, Nov. 1988.

[24] P.M.Goggans, and T.H.Shumpert, "Backscatter RCS for TE and TM Excitations of Dielectric-Filled Cavity Backed Apertures in 2-D Bodies", *IEEE Trans. Antennas Propagat.,* vol. 39, No.8, pp. 1224-1227, Aug. 1991.

[25] J. A. Beren, "Diffraction of an H-Polarized Electromagnetic Wave by a Circular Cylinder with an Infinite Axial Slot," *IEEE Trans. Antennas Propagat.,* vol AP-31, pp. 419-425, May 1983.

[26] M. Abramowitz and I. A. Stegun, *Handbook of Mathematical Functions.* New York:Dover, 1965

[27] S. Steigberg, "Meromorphic Families of Compact Operators," *Arch. Rational Mech. Anal.,* vol. 31, No 5, pp. 372-379,1968

[28] R. F. Harrington, *Time-Harmonic Electromagnetic Fields* New York: McGraw-Hill Book Company, 1961

[29] F. D. Gakhov, *Boundary Value Problems*, Elmsford, New York: Pergamon, 1966

[30] P. M. Morse and H. Feshbach, *Methods of Theoretical Physics,* vol 1. New York: McGraw-Hill, 1953, sec. 8.2, pp. 907–925.

[31] P. J. Clarricoats, P. E. Green and A. A. Oliver, "Slot-mode Propagation in Rectangular Waveguide," *Electronics Lett.*, vol.2, pp. 307-308, 1966

[32] E. I. Veliev, A. I. Nosich, and V. P. Shestopalov, "Propagation of Electromagnetic Waves in a Cylindrical Waveguide with a Longitudinal Slit", *Radio Eng. Electron. Physics*, Engl. Transl., vol. 22, pp. 29-35, 1977.

[33] L. Rayleigh, "Theory of Helmholtz Resonator," *Proc. Royal Soc. London (A),* vol. 92, pp. 265-275, 1915.